Benchmarks for higher-order modes evaluation in the free vibration response of open thin-walled beams due to the cross-sectional deformations

Benchmarks for higher-order modes evaluation in the free vibration response of open thin-walled beams due to the cross-sectional deformations

Xiangyang Xu[a,*], Erasmo Carrera[b,†], Riccardo Augello[b,‡], Ehsan Daneshkhah[b,§], Hao Yang[a,]

[a]School of rail transportation, Soochow University, Suzhou, China

[b]Mul^2 Group, Department of Mechanical and Aerospace Engineering, Politecnico di Torino, 10129 Torino, Italy

Abstract:

Highly flexible thin-walled beams with complex open cross-sections are sensitive to torsional and warping effects. The analysis of higher-order vibration modes in these structures needs more accurate and precise methods in order to achieve reliable results and detect the cross-sectional deformations in the structures' free vibration response. This paper analyzes higher vibration modes in a series of thin-walled beams, which were proposed by Chen as benchmark problems. These are all open-section thin-walled beams with complex geometries. Global vibration modes, such as bending and torsion, related to the rigid cross-sectional deformations can be detected via classical and shear refined theories. However, cross-sectional deformations appear at higher frequencies, and these modes are mixed with the global ones. To highlight this fact, this paper compares classical beam theories with refined ones based on the Carrera Unified Formulation (CUF) and the shell results using the commercial finite element (FE) software and the data available from the literature. The CUF FEs based on the power of cross-sectional deformation coordinates (x, z) and those based on the Lagrangian polynomials are implemented and compared using Modal Assurance Criterion. A number of interesting conclusions are drawn about the effectiveness of classical and CUF-based results. The need for models capable of detecting cross-sectional deformations is outlined. In fact, many modes are lost by classical beam theories; on the other hand, they show rigid cross-section modes that do not really exist. This fact is also confirmed by the shell models, which are more expensive in terms of computational costs regarding the efficient CUF ones proposed here.

Keywords: Free vibration analysis; Carrera Unified Formulation; Thin-walled beam structures; higher-order modes, cross-sectional deformations.

1 Introduction

Lightweight thin-walled beam structures with open sections are used extensively in different engineering applications and industries, such as aerospace and construction. Beams are structures having one dimension much larger than the other two and primarily subjected to lateral loads, resulting in the bending of their reference axes. A general beam should be able to sustain extension, compression, bending, transverse shear (flexure) and twisting loads [1]. One-dimensional beam theories

*Full Professor. Email: x.y.xu@suda.edu.cn

†Full Professor. E-mail: erasmo.carrera@polito.it

‡Ph.D. student. E-mail: riccardo.augello@polito.it

§Ph.D. student. E-mail: ehsan.daneshkhah@polito.it

have been studied broadly because of the simplicity and lower computational costs. Beam theories were initially developed by Euler [2], Bernoulli [3], Timoshenko [4, 5] and further by Vlasov for the thin-walled beams [6, 7].

Free vibration occurs when a system is left to vibrate on its own after the initial excitation. There are no external forces acting on the system in the free vibration [8]. The free vibration response of beam structures has been analyzed by many researchers [9, 10, 11]. Comprehensive studies were presented in books by Gorman [12], and Blevins [13]. The free vibration analysis of stepped beams is investigated in some research papers [14, 15, 16, 17]. Li [18] presented an approach for the free vibration analysis of generally supported beams, considering the displacement of the beam as a combination of Fourier series and auxiliary polynomial function. Chen and Hsiao [19] developed an FE method for the coupled free vibration of thin-walled beams with open cross-sections, and investigated numerical examples from the literature [20, 21, 22]. Dey and Talukdar [23] worked on the free vibration of the thin-walled channel section steel beam and compared FE and experimental results. Murin et al. investigated the effect of torsional warping on the eigenvibrations of thin-walled beams with functionally graded materials [24]. One of the best contribution on the topic is represented by the Generalized Beam Theory (GBT). It was introduced by Schardt [25] and further developed by Camotim and Silvestre [26, 27, 28] and was efficiently used for the analysis of vibrations in many thin-walled structures. Kugler et al. [29, 30] proposed a novel GBT based on the reference beam problem for the slender prismatic structures. Piana et al. [31] compared the experimental and numerical results in a compressed non-symmetric thin-walled beam with a cruciform cross-section. They obtained the natural frequencies of the beam exciting the specimen by means of a hammer. They detected the frequencies by using the Peak Picking technique using the PZT pickups or Laser sensors. A finite element commercial code was used to validate the frequencies, and a finite differences code was developed to follow the frequency-load responses. Jrad presented a comprehensive study on the dynamic behavior of thin-walled beams using experimental, numerical and analytical approaches [32, 33]. Fazzolari [34] proposed a Ritz formulation for the free vibration analysis of thin-walled structures.

In many cases, the beam and plate structures are subjected to high frequencies and large amplitude vibrations. Hence, the higher modes in the free vibration analysis of structures have been investigated in some studies. A review paper was presented by Langley and Bardell [35] on the alternative analysis methods for high frequency vibrations of aerospace structures. Wei et al. [36] introduced a discrete singular convolution algorithm for the high frequency vibrations of structures. Sudalagunta et al. [37] provided a scheme for higher modes of vibrations for one-dimensional structures based on the classic Ritz method. Ding et al. [38] considered the displacements of trigonometric function and presented a theory for high frequency vibrations of rectangular beams. Lin et al. [39] derived an energy FE formulation for the high frequency vibration of beam structures. Wang [40] proposed a novel discrete singular convolution algorithm for the high frequency vibration of structures and solved some free vibration problems of beam and plate structures.

In essence, it can be pointed out that when the problem is not governed by higher-order phenomena, a 2D description of the problem (as provided, for instance, by GBT) is efficient, in terms of efforts spent. On the contrary, when the problem is governed by complex phenomena, a 3D description of the problem is mandatory. In this paper, this approach is used employing the Carrera Unified Formulation (CUF). CUF was introduced as a promising and reliable method for the free vibration analysis of plate and shell structures [41, 42, 43, 44]. Carrera et al. [45] presented a hierarchical FE based on the CUF for the free vibration response of beam structures. They formulated the mass and stiffness matrices of the structure in terms of the independent fundamental nuclei. Carrera et al. [46] evaluated higher-order theories using the framework of the CUF for the free vibration response of various beam cross-sections, such as rectangular, rectangular thin-walled, C-shaped, and annular beams. Petrolo et al. [47] conducted a free vibration analysis of compact and bridge-like cross-sections using the CUF framework. Pagani et al. [48] used the higher-order kinematic field based on the CUF, and presented an exact dynamic stiffness formulation for the free

vibration analysis of thin-walled structures. Pagani et al. [49] investigated the effect of nonstructural localized inertia on the free vibration analysis of thin-walled structures by opportunely modifying the fundamental nucleus of the mass matrix. Pagani et al. [50] applied radial basis functions to the free vibration analysis of thin-walled beams. Dan et al. [51] worked on the free vibration of simply supported beams with solid and thin-walled cross-sections using the CUF. Xu et al. [8] presented an FE method based on the CUF by using Lagrange polynomial expansion for thin-walled beams with different cross-sections.

Higher vibration modes of thin-walled beams with complex geometries are investigated in this paper by using the framework of CUF. This paper analyzes higher vibration modes in a series of thin-walled beams, which were proposed by Chen as benchmark problems. Classical and higher-order beam theories are used, and the effect of cross-sectional deformations in the higher-order modes are investigated. The Modal Assurance Criterion (MAC) is used to compare the free vibration modes based on different structural theories. A comprehensive comparison is presented between the classical beam theories, refined ones based on the CUF, shell results from the commercial FE software and the data available from the literature. It is shown that many modes are lost by classical beam theories, and instead, they show rigid-cross section modes that do not really exist. It is also confirmed that by using the CUF, the results are not only obtained in a very cost-effective manner but they are also accurate and in agreement with shell models with high computational costs.

2 Preliminary considerations

If we consider a generic beam with the cross-section domain S in the $x-z$ plane, and the axis along the y direction, the displacement, stress, and the strain vectors are defined as the following vectorial forms:

$$\begin{aligned} \boldsymbol{u}(x,y,z;t) &= \{u_x\, u_y u_z\}^T \\ \boldsymbol{\sigma} &= \{\sigma_{xx}\ \ \sigma_{yy}\ \ \sigma_{zz}\ \ \sigma_{xz}\ \ \sigma_{yz}\ \ \sigma_{xy}\}^T \\ \boldsymbol{\varepsilon} &= \{\varepsilon_{xx}\ \ \varepsilon_{yy}\ \ \varepsilon_{zz}\ \ \varepsilon_{xz}\ \ \varepsilon_{yz}\ \ \varepsilon_{xy}\}^T \end{aligned} \tag{1}$$

If the small displacements and rotations are considered, the geometrical relations between the strains and the displacements are expressed in the matrix forms as follows.

$$\boldsymbol{\epsilon} = \boldsymbol{D}\,\mathbf{u} \tag{2}$$

where $\boldsymbol{D}$ is the linear differential operators defined as:

$$\boldsymbol{D} = \begin{bmatrix} \partial_x & 0 & 0 \\ 0 & \partial_y & 0 \\ 0 & 0 & \partial_z \\ \partial_z & 0 & \partial_x \\ 0 & \partial_z & \partial_y \\ \partial_y & \partial_x & 0 \end{bmatrix}, \tag{3}$$

where $\partial_x = \dfrac{\partial(\cdot)}{\partial x}$, $\partial_y = \dfrac{\partial(\cdot)}{\partial y}$, and $\partial_z = \dfrac{\partial(\cdot)}{\partial z}$ are partial derivative operators.

Based on the Hook's law, the stress-strain relationship is:

$$\boldsymbol{\sigma} = \boldsymbol{C}\,\boldsymbol{\epsilon} \tag{4}$$

For the isotropic material, the matrix $\boldsymbol{C}$ is

$$\boldsymbol{C} = \begin{bmatrix} \lambda+2G & \lambda & \lambda & 0 & 0 & 0 \\ \lambda & \lambda+2G & \lambda & 0 & 0 & 0 \\ \lambda & \lambda & \lambda+2G & 0 & 0 & 0 \\ 0 & 0 & 0 & G & 0 & 0 \\ 0 & 0 & 0 & 0 & G & 0 \\ 0 & 0 & 0 & 0 & 0 & G \end{bmatrix} \tag{5}$$

where G and λ are the Lame's parameters related to the properties of isotropic material, and one can use $G = E/(2(1+\nu))$ and $\lambda = \nu E/((1+\nu)(1-2\nu))$ in case of Poisson's ratio and Young's modulus [49].

3 Carrera Unified Formulation for the free vibration analysis

The three-dimensional displacement field according to the Carrera Unified Formulation (CUF) for the beam structures is [52]:

$$\boldsymbol{u}(x,y,z;t) = F_\tau(x,z)\,\boldsymbol{u}_\tau(y;t), \qquad \tau = 0,1,\cdots,N, \tag{6}$$

where F_τ is the set of cross-section functions and $\boldsymbol{u}_\tau$ is the generalized displacement vector. As it is clear from Eq. (6), the use of CUF provides us a great advantage of arbitrarily selecting the expansions of any order over the beam cross-section. Therefore, different structural theories based on the order of expansion could be implemented and used. In this research, Taylor and Lagrange cross-section functions are used to model the beam structure. By using the finite element approximation, the displacement vector $\boldsymbol{u}_\tau$ based on the nodal parameters $\boldsymbol{u}_{\tau i}$ and shape functions N_i is defined as:

$$\boldsymbol{u}_\tau(y;t) = N_i(y)\,\boldsymbol{q}_{\tau i}(t), \qquad i = 1,2,\ldots,p+1, \tag{7}$$

where N_i is the i-th shape function, p is related to the order of the shape functions and $\mathbf{q}$ is vector of the nodal unknowns. More information about the Lagrange polynomials and shape functions can be found in [53]. By using the finite element approximation and the CUF, the displacement field can be expressed as:

$$\boldsymbol{u}(x,y,z;t) = N_i(y)\,F_\tau(x,z)\,\boldsymbol{q}_{\tau i}(t) \tag{8}$$

According to the Principle of Virtual Displacements (PVD), we have:

$$\delta L_{\text{int}} \;+\; \delta L_{\text{ine}} \;=\; \delta L_{ext} \tag{9}$$

where L_{int}, L_{ine}, and L_{ext} represent the strain energy, work of the inertial loadings, and the work of external loadings. For the free vibration analysis, the work of external loadings is zero, therefore:

$$\delta L_{\text{int}} \;+\; \delta L_{\text{ine}} \;=\; 0 \tag{10}$$

By using the CUF as introduced previously, the following equations are obtained for the virtual variations of strain energy and the inertial work.

$$\begin{aligned} \delta L_{\text{int}} &= \int_v \delta\boldsymbol{\varepsilon}^T\boldsymbol{\sigma}\,dV = \delta\boldsymbol{u}_{sj}^T\left(\int_V F_s(x,z)N_j(y)\boldsymbol{D}^T\boldsymbol{C}\boldsymbol{D}N_i(y)F_\tau(x,z)dV\right)\boldsymbol{u}_{\tau i} = \delta\boldsymbol{u}_{sj}^T\boldsymbol{K}^{\tau sij}\boldsymbol{u}_{\tau i} \\ \delta L_{\text{ine}} &= \int_v \delta\boldsymbol{u}^T\rho\ddot{\boldsymbol{u}}dV = \delta\boldsymbol{u}_{sj}^T\left(\int_V F_s(x,z)N_j(y)\rho N_i(y)F_\tau(x,z)dV\right)\ddot{\boldsymbol{u}}_{\tau i} = \delta\boldsymbol{u}_{sj}^T\boldsymbol{M}^{\tau sij}\ddot{\boldsymbol{u}}_{\tau i} \end{aligned} \tag{11}$$

where $\boldsymbol{K}^{\tau sij}$ and $\boldsymbol{M}^{\tau sij}$ are the Fundamental Nuclei (FN) of the stiffness and mass matrices. These are 3×3 matrices based on the unified formulation for a given i, j pair, and independent of the order of the structure model with a fixed form. The repeated indexes indicate summation. The

global matrices are obtained by considering all the combinations of the indices i, j, τ, and s. More details about the fundamental nucleus formulation and their explicit forms can be found in [52, 54].

If we substitute the virtual variations of strain energy and the inertial work from Eqs. (11) into Eq. (10), the PVD could be written in the following form:

$$\delta \boldsymbol{u}_{sj}^{T}(\boldsymbol{K}^{\tau sij}\boldsymbol{u}_{\tau i} + \boldsymbol{M}^{\tau sij}\ddot{\boldsymbol{u}}_{\tau i}) = 0 \tag{12}$$

That could be expressed as:

$$\boldsymbol{M}^{\tau sij}\ddot{\boldsymbol{u}}_{\tau i} + \boldsymbol{K}^{\tau sij}\boldsymbol{u}_{\tau i} = 0 \tag{13}$$

Due to the fact that the problem is linear, the harmonic solutions can be used in order to obtain the natural frequencies; therefore, the eigenvalues problem can be solved as follows.

$$(-\omega_k^2\boldsymbol{M} + \boldsymbol{K})\boldsymbol{u}_k = 0 \tag{14}$$

where ω_k are the natural frequencies, and $\boldsymbol{u}_k$ is the k th eigenvector.

3.1 Refined Taylor Expansion

Taylor Expansion (TE) models are formulated by employing polynomial expansion of the kind $x^m z^n$ as cross-section function F_τ. It should be noted that m and n are positive integers. The order of TE model (N) represents the structural theory of the beam, and is defined as a user input. For instance in the case of $N = 2$, the second-order displacement field is:

$$\begin{aligned} u_x &= u_{x_1} + xu_{x_2} + zu_{x_3} + x^2u_{x_4} + xzu_{x_5} + z^2u_{x_6} \\ u_y &= u_{y_1} + xu_{y_2} + zu_{y_3} + x^2u_{y_4} + xzu_{y_5} + z^2u_{y_6} \\ u_z &= u_{z_1} + xu_{z_2} + zu_{z_3} + x^2u_{z_4} + xzu_{z_5} + z^2u_{z_6} \end{aligned} \tag{15}$$

where u_{x_1} to u_{z_6} are the eighteen generalized displacement variables. In Fig. 1 some of theses variables are shown schematically for a beam example under bending around z axis according to the linear TE model ($N = 1$). As can be seen in this figure, for the mentioned beam example u_{x_1} is the displacement and u_{y_2} is the rotation. The classical beam theories such as Euler–Bernoulli beam theory (EBBT) and Timoshenko beam theory (TBT) can be obtained as particular cases of the linear TE model [52]. For instance, the TBT considers only the following terms for the displacement field:

$$\begin{aligned} u_x &= u_{x_1} \\ u_y &= u_{y_1} + xu_{y_2} + zu_{y_3} \\ u_z &= u_{z_1} \end{aligned} \tag{16}$$

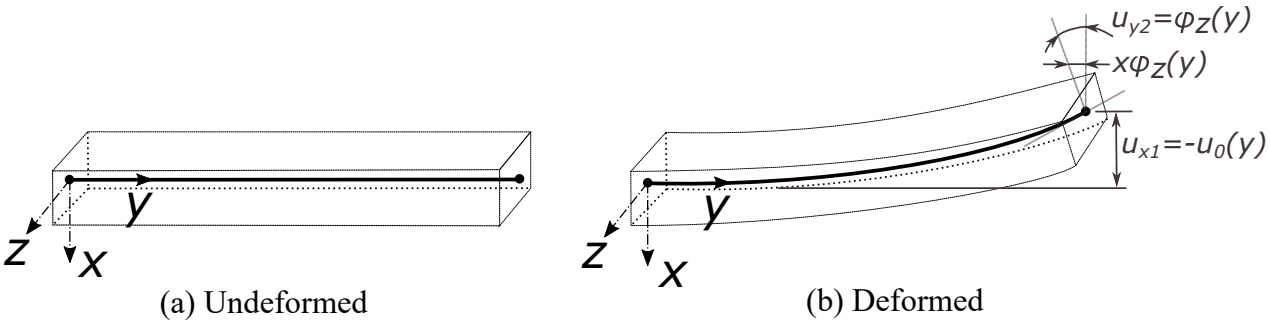

Figure 1: Some of the generalized displacement variables based on the linear TE model for a schematic beam under bending around z axis

3.2 Refined Lagrange Expansion

Lagrange Expansions (LE) have been demonstrated to be very effective for several applications, including aerospace and civil structures [55, 56, 57, 58]. For the LE models, the unknown variables are pure displacements (See Fig. 2). In this research paper, different numbers of nine-nodes Lagrange polynomials (L9) are adopted for the expansion function over the cross-section. By using the isoparametric formulation for the beams with arbitrary cross-sections, the interpolation functions and the coordinates of the points for the L9 Lagrange polynomials are mentioned in Eqs. (17) and Table 1, respectively. Fig. 3 shows the L9 Lagrange elements in the actual and normalized geometries. Interested readers are referred to the book by Carrera et al. for more information about the beam models with LE [52].

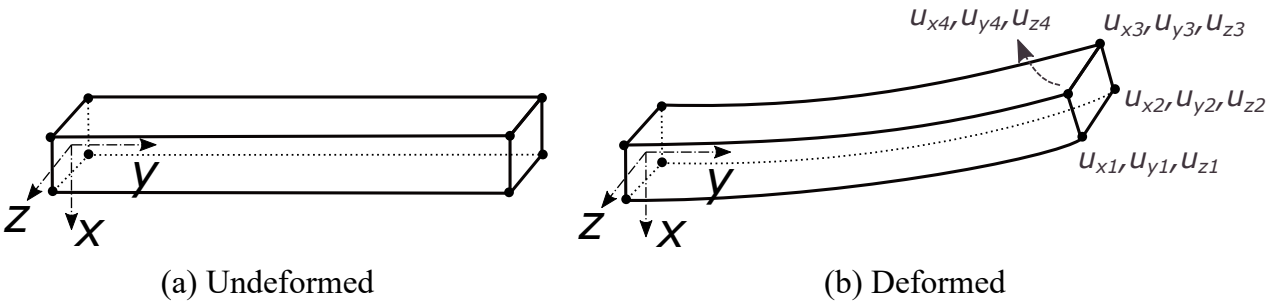

(a) Undeformed (b) Deformed

Figure 2: Pure displacement variables based on the Lagrange model with four points for a schematic beam under bending around z axis

Some of the generalized displacement variables based on the linear TE model for a schematic beam under bending around z axis

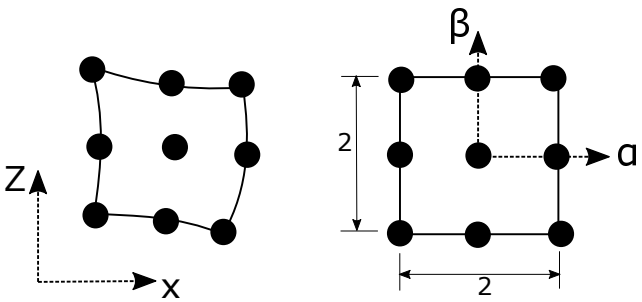

Figure 3: Nine nodes Lagrange polynomials in the actual and normalized geometry

where

$$F_\tau = \tfrac{1}{4}(\alpha^2 + \alpha\alpha_\tau)(\beta^2 + \beta\beta_\tau), \qquad \tau = 1,3,5,7$$

$$F_\tau = \tfrac{1}{2}\beta_\tau^2(\beta^2 + \beta\beta_\tau)(1-\alpha^2) + \tfrac{1}{2}\alpha_\tau^2(\alpha^2 + \alpha\alpha_\tau)(1-\beta^2), \qquad \tau = 2,4,6,8 \tag{17}$$

$$F_\tau = (1-\alpha^2)(1-\beta^2), \qquad \tau = 9$$

and

Table 1: Normalized coordinates of L9 element

Points	1	2	3	4	5	6	7	8	9
α_τ	-1	0	1	1	1	0	-1	-1	0
β_τ	-1	-1	-1	0	1	1	1	0	0

3.3 Shear locking

A numerical phenomenon that may occur as the thickness of beams or plates decreases is shear locking [59, 60]. This arises because of the overestimation of the shear stiffness of the structures that tends to be infinite as the thickness tends to zero [52]. Some techniques to tackle this issue are reduced, selective integration, and Mixed Interpolation of Tensorial Components (MITC).

Zienkiewicz [61, 62] proposed the reduced integration method that suggests the decrease of the order of numerical integration in some terms of the stiffness matrix in order to reduce the stiffness of displacement-based elements. Selective integration [63, 64] is another technique based on the reduced integration for transverse shear terms. Note that in the selective integration method, a full quadrature is considered for the other terms of the stiffness matrix. In fact, this method is based on a reduced Gauss integration of the terms of the stiffness matrix that are related to the shear. Therefore, due to the reduction of the number of Gauss points, the shear stiffness of structure is also decreased. The Mixed Interpolation of Tensorial Components (MITC) [65, 66] is also a remarkable and successful method for eliminating the shear locking phenomenon. In the MITC formulation, an independent FE approximation is introduced into the element domain for the transverse shear strains. This results in the elimination of the transverse shear locking phenomenon. This method is based on the use of assumed strain distributions for the derivation of the transverse shear terms and, eventually membrane terms of the stiffness matrix of the finite elements[67]. In this paper, the MITC method is used in combination with the CUF one-dimensional formulation. Interested readers are referred to the work by Carrera [67] for more information about the formulation and extension of MITC methodology to higher-order and hierarchical beam theories.

4 Description of the Chen benchmark

In this section, a series of thin-walled beams with open cross-sections proposed by Chen [19] as benchmark problems are introduced. The first two thin-walled beams are with C-shaped and T-shaped cross-sections. The other two thin-walled beams are with arbitrary and complex cross-sections. For each beam, the cross-section geometries and isotropic material properties are illustrated in Fig. 4. Note that all the dimensions in this figure are in millimeters (mm).

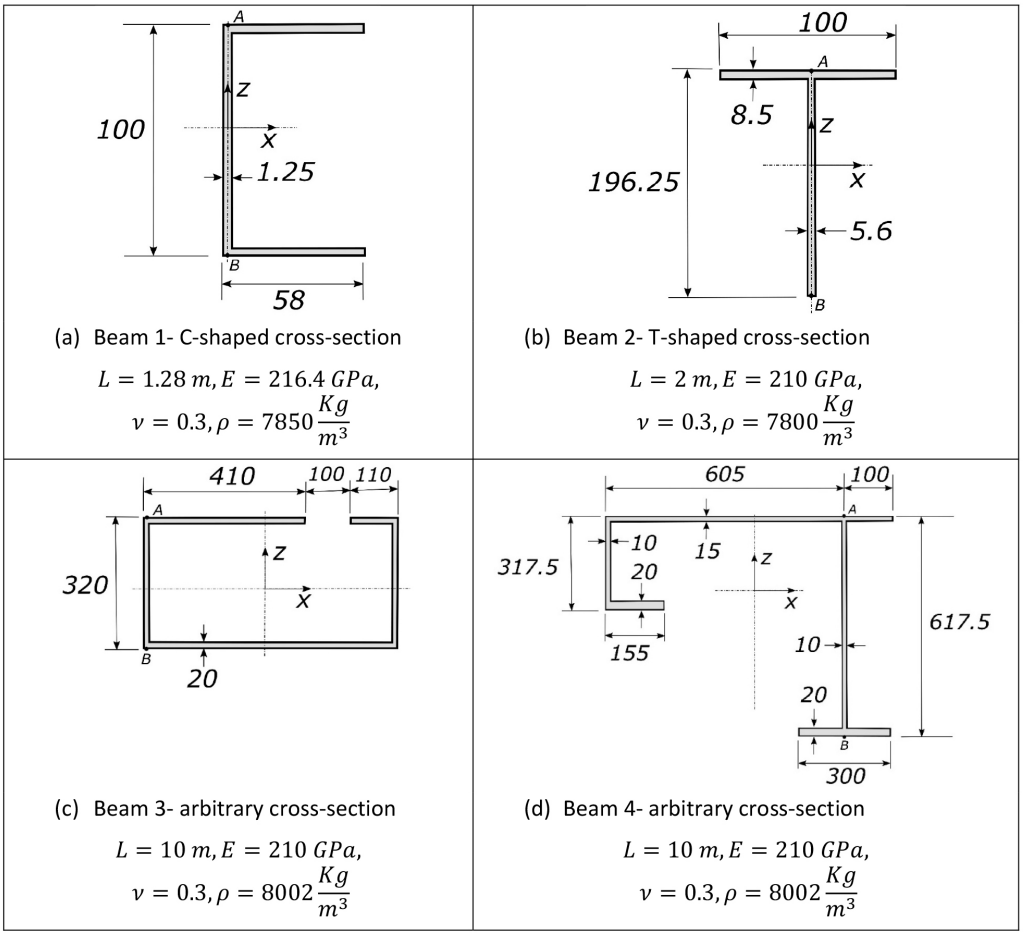

Figure 4: The schematic view and material properties of the beam 1- C-shaped cross-section

5 Numerical Assessments

In this section, the convergence study is performed in order to evaluate the effect of number of FEs and different expansions over the beam cross-section. Afterwards, the shear locking behavior is investigated for some of the beams, and the efficiency of methods for eliminating the shear locking is evaluated.

5.1 Convergence study

In this section, the convergence analysis is presented based on the displacements and axial stresses for the cantilever beams subjected to a point load at the free end. The displacements at the free end of the beam, and the axial stresses near the clamped edge of the beam are evaluated. Four beams with C-shaped, T-shaped, and two arbitrary cross-sections are investigated.

5.1.1 Beam 1- C-shaped cross-section

In order to investigate the effect of FE discretization, a convergence study is conducted for the displacements and stresses of the C-shaped beam. The beam is clamped at one end and subjected to a downward tip force $P = 1000N$ at the free end (point A in Fig. 4(a)). The results of the vertical displacements at the bottom point (See point B of Fig. 4(a), $y = 1280mm$) and axial compressive stresses at the bottom point ($y = 128mm$) of the C-shaped beam are reported in Table 2. The results of this table are presented for the beam elements with two nodes (B2), three nodes (B3), and four nodes (B4) elements, respectively. 14 Lagrange polynomials with nine nodes (14L9) are used for

the expansion function over the cross-section. The last columns of table 2 are devoted to the error values of displacements and axial stresses compared to the 20B4-14L9 model. Based on the values of this table, Figs. 5a and 5b, which indicate the displacements and axial stress versus the DOF of each model. In addition, the corresponding error values are plotted in Figs. 5c and 5d. The results show that for both the vertical displacements and axial stresses, the convergence rate of B4 beam elements is significantly higher than B3 and B2 elements. Furthermore, the predicted displacement values for B2 elements are not accurate enough because of the necessity of the consideration of shear refinements in the model. This issue will be further investigated in Section 5.2.

Table 2: The convergence analysis of the vertical displacements at the bottom point (See point B of Fig. 4(a), $y = 1280mm$) and axial compressive stresses at the bottom point ($y = 128mm$) of the beam 1- C-shaped cross-section- effect of FE discretization

Model	DOF	Displacement (mm)	Axial Stress (MPa)	Displacement Error %	Axial Stress Error %
5B2-14L9	1566	3.29	64.36	78.84	77.29
10B2-14L9	2871	6.48	87.13	58.32	69.26
20B2-14L9	5481	10.72	213.14	31.06	24.81
30B2-14L9	8091	12.80	235.51	17.68	16.92
50B2-14L9	13311	14.38	263.54	7.52	7.03
5B3-14L9	2871	15.10	139.42	2.89	50.81
10B3-14L9	5481	15.37	220.11	1.15	22.35
20B3-14L9	10701	15.49	272.46	0.38	3.88
30B3-14L9	15921	15.53	281.03	0.12	0.86
5B4-14L9	4176	15.36	187.63	1.22	33.81
10B4-14L9	8091	15.49	237.92	0.38	16.07
20B4-14L9	15921	15.55	283.48	0.00	0.00

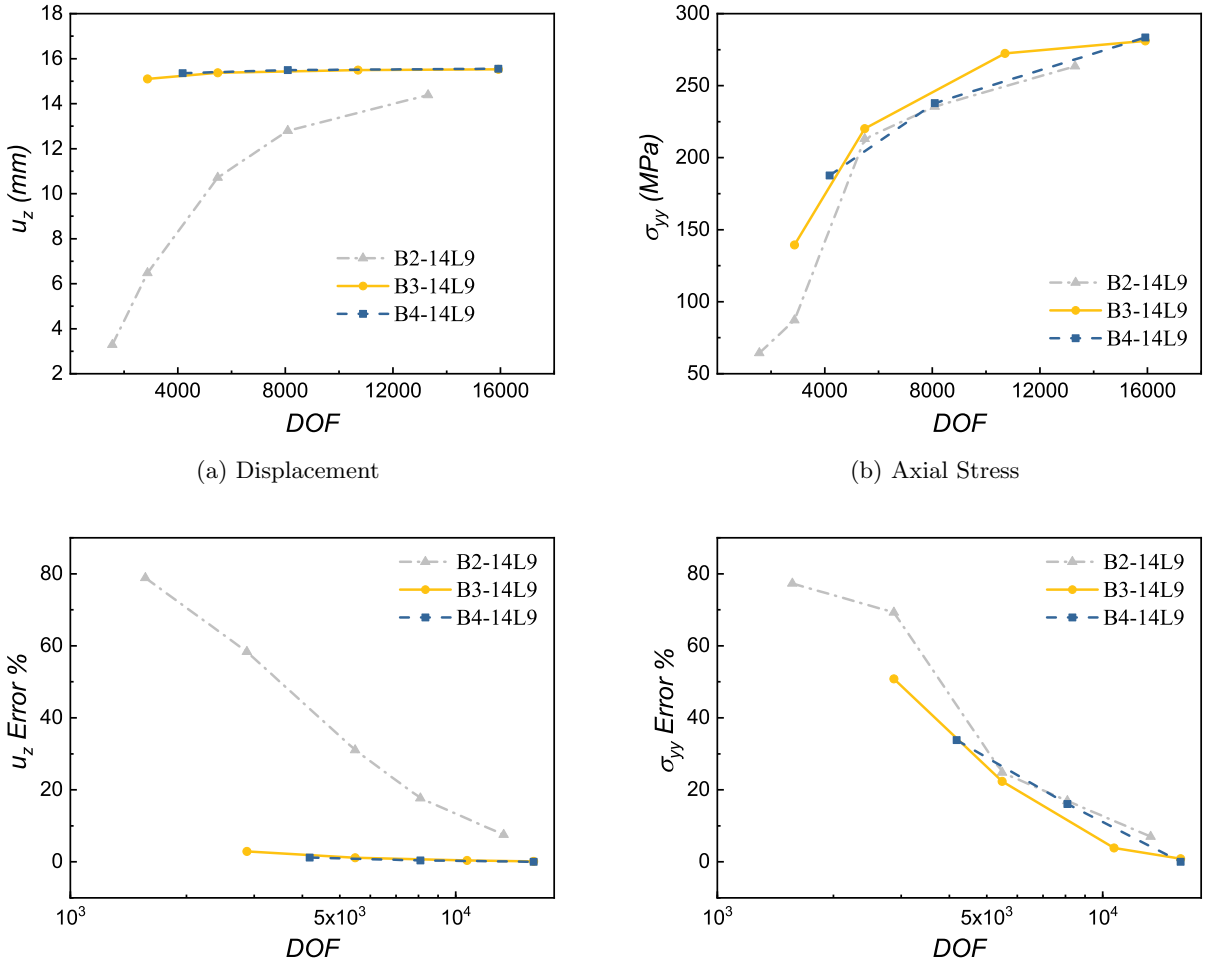

(a) Displacement

(b) Axial Stress

(c) Displacement Error

(d) Axial Stress Error

Figure 5: The convergence analysis of the vertical displacements at the bottom point (See point B of Fig. 4(a), $y = 1280mm$) and axial compressive stresses at the bottom point ($y = 128mm$) of the beam 1- C-shaped cross-section- effect of FE discretization

In order to investigate the effect of structural theories, the same convergence study is conducted for the displacements and stresses of the C-shaped beam. Three LE models of 8L9, 14L9, and 22L9 are considered with 20B4 FE beams. As shown in Fig. 6, these LE models include 51, 87, and 135 Lagrange points, respectively. In addition, five TE models of order 1, 2, 5, 10, and 15 are considered for the sake of completeness. The results of this convergence analysis are reported in Table 3, where the last two columns are related to the errors of displacements and axial stresses in comparison with the 20B4-22L9 model. The results reveal that classical and TE models of lower orders cannot predict the displacements and axial stresses accurately. For instance, consider the cases of $TE = 1$ and $TE = 2$ that show more than 50 percent error in comparison with the refined model of 22L9. Thus, the selection of fine structural theories is vital for the accurate evaluation of displacements and stresses in the beams with unsymmetric cross-sections under bending and torsion.

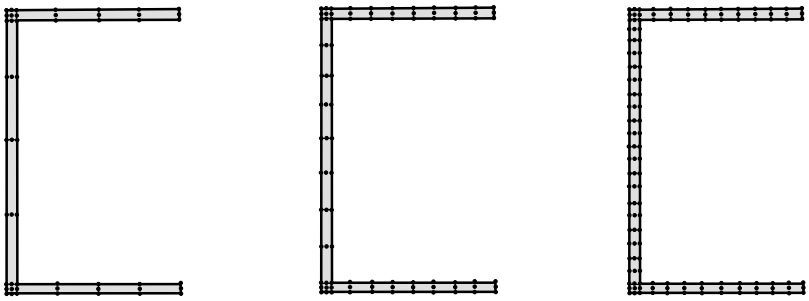

Figure 6: Discretization of the beam-1 cross-section based on different Lagrange expansions

Table 3: The convergence analysis of the vertical displacements at the bottom point (See point B of Fig. 4(a), $y = 1280mm$) and axial compressive stresses at the bottom point ($y = 128mm$) of the beam 1- C-shaped cross-section- effect of the structural theory

Model	DOF	Displacement (mm)	Axial Stress (MPa)	Displacement Error %	Axial Stress Error %
20B4,TE=1	549	7.24	127.98	53.44	54.88
20B4,TE=2	1098	7.18	128.60	53.82	54.66
20B4,TE=5	3843	8.31	155.63	46.55	45.13
20B4,TE=10	12078	14.63	267.55	5.91	5.67
20B4,TE=15	24888	15.33	277.15	1.41	2.29
20B4-8L9	933	15.54	283.29	0.06	0.12
20B4-14L9	15921	15.55	283.48	0.00	0.05
20B4-22L9	24705	15.55	283.65	0.00	0.00

5.1.2 Beam 2- T-shaped cross-section

In order to investigate the effect of FE discretization, a convergence study is conducted for the displacements and stresses of the T-shaped beam. The beam is clamped at one end and subjected to a downward tip force $P = 15000N$ at the free end (point A in Fig. 4(b)). The results of the vertical displacements at the bottom point (See point B of Fig. 4(b), $y = 2000mm$) and axial compressive stresses at the bottom point ($y = 200mm$) of the T-shaped beam are reported in Table 4. The results of this table are presented for the beam elements with two nodes (B2), three nodes (B3), and four nodes (B4) elements, respectively. 15 Lagrange polynomials with nine nodes (15L9) are used for the expansion function over the cross-section. The last columns of table 4 are devoted to the error values of displacements and axial stresses compared to the 20B4-15L9 model.

Table 4: The convergence analysis of the vertical displacements at the bottom point (See point B of Fig. 4(b), $y = 2000mm$) and axial compressive stresses at the bottom point ($y = 200mm$) of the beam 2- T-shaped cross-section- effect of FE discretization

Model	DOF	Displacement (mm)	Axial Stress (MPa)	Displacement Error %	Axial Stress Error %
5B2-15L9	1674	10.84	228.88	57.10	53.57
10B2-15L9	3069	18.82	327.71	25.52	33.52
20B2-15L9	5859	23.20	474.24	8.19	3.79
30B2-15L9	8649	24.28	475.76	3.91	3.48
50B2-15L9	14229	24.90	486.85	1.46	1.23
5B3-15L9	3069	24.84	402.06	1.70	18.43
10B3-15L9	5859	25.10	441.04	0.67	10.53
20B3-15L9	11439	25.22	486.00	0.19	1.41
30B3-15L9	17019	25.26	489.21	0.03	0.76
5B4-15L9	4464	25.09	429.61	0.71	12.85
10B4-15L9	8649	25.22	467.26	0.19	5.21
20B4-15L9	17019	25.27	492.96	0.00	0.00

In order to investigate the effect of structural theories, the same convergence study is conducted for the displacements and stresses of the T-shaped beam. Three LE models of 9L9, 15L9, and 23L9 are considered with 20B4 FE beams. As shown in Fig. 7, these LE models include 57, 93, and 141 Lagrange points, respectively. In addition, five TE models of order 1, 2, 5, 10, and 15 are considered for the sake of completeness. The results of this convergence analysis are reported in Table 5, where the last two columns are related to the errors of displacements and axial stresses in comparison with the 20B4-23L9 model. The results reveal that in contradiction with the previous beam example, for the T-shaped beams, classical and TE models of lower orders can also predict the displacements and axial stresses accurately. For instance, consider the cases of $TE = 1$ and $TE = 2$ that show less than 1 percent error in comparison with the refined model of 23L9. This is due to the effect of the geometry of cross-section and the applied load point. In fact, for this example, the load is applied at the midline of the cross-section where there are symmetric geometric conditions with respect to the z direction. Therefore, the torsional effects are reduced, and that results in the capability of classical and low order models for capturing the accurate values of displacements and axial stresses.

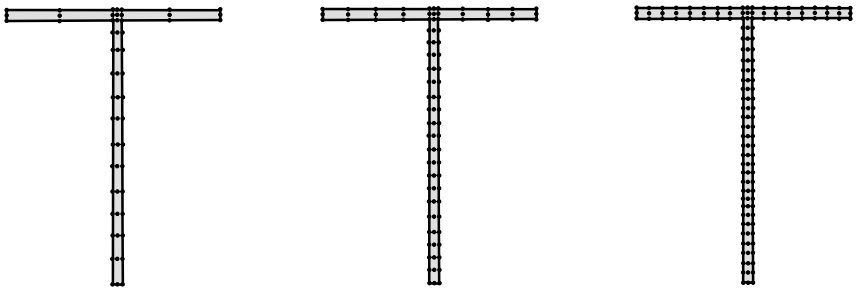

Figure 7: Discretization of the beam-2 cross-section based on different Lagrange expansions

Table 5: The convergence analysis of the vertical displacements at the bottom point (See point B of Fig. 4(b), $y = 2000mm$) and axial compressive stresses at the bottom point ($y = 200mm$) of the beam 2- T-shaped cross-section- effect of the structural theory

Model	DOF	Displacement (mm)	Axial Stress (MPa)	Displacement Error %	Axial Stress Error %
20B4,TE=1	549	25.18	488.11	0.35	0.90
20B4,TE=2	1098	25.09	489.93	0.71	0.53
20B4,TE=5	3843	25.25	491.95	0.07	0.12
20B4,TE=10	12078	25.27	492.54	0.07	0.00
20B4,TE=15	24888	25.27	492.58	0.00	0.00
20B4-9L9	10431	25.27	493.68	0.00	0.22
20B4-15L9	17019	25.27	492.96	0.00	0.08
20B4-23L9	25803	25.27	492.56	0.00	0.00

5.1.3 Beam 3- Arbitrary cross-section

In order to investigate the effect of FE discretization, a convergence study is conducted for the displacements and stresses of the beam 3 with arbitrary cross-section. The beam is clamped at one end and subjected to a downward tip force $P = 30000N$ at the free end (point A in Fig. 4(c)). The results of the vertical displacements at the bottom point (See point B of Fig. 4(c), $y = 10000mm$) and axial compressive stresses at the bottom point ($y = 1000mm$) of the beam are reported in Table 6. The results of this table are presented for the beam elements with two nodes (B2), three nodes (B3), and four nodes (B4) elements, respectively. 16 Lagrange polynomials with nine nodes (16L9) are used for the expansion function over the cross-section. The last columns of table 6 are devoted to the error values of displacements and axial stresses compared to the 20B4-16L9 model.

Table 6: The convergence analysis of the vertical displacements at the bottom point (See point B of Fig. 4(c), $y = 10000mm$) and axial compressive stresses at the bottom point ($y = 1000mm$) of the beam 3- arbitrary cross-section- effect of FE discretization

Model	DOF	Displacement (mm)	Axial Stress (MPa)	Displacement Error %	Axial Stress Error %
5B2-16L9	1782	14.60	10.83	82.56	85.92
10B2-16L9	3267	33.92	27.51	59.48	64.25
20B2-16L9	6237	58.88	59.05	29.67	23.27
30B2-16L9	9207	70.00	66.13	16.39	14.07
50B2-16L9	15147	78.06	72.98	6.77	5.17
5B3-16L9	3267	82.13	39.04	1.91	49.27
10B3-16L9	6237	83.14	69.22	0.70	10.05
20B3-16L9	12177	83.56	74.97	0.20	2.58
30B3-16L9	18117	83.68	76.76	0.05	0.25
5B4-16L9	4752	83.10	47.93	0.75	37.72
10B4-16L9	9207	83.53	71.06	0.23	7.66
20B4-16L9	18117	83.73	76.96	0.00	0.00

In order to investigate the effect of structural theories, the same convergence study is conducted for the displacements and stresses of the beam 3 with arbitrary cross-section. Three LE models of 12L9, 16L9, and 25L9 are considered with 20B4 FE beams. As shown in Fig. 8, these LE models include 75, 99, and 153 Lagrange points, respectively. In addition, five TE models of order 1, 2, 5, 10, and 15 are considered for the sake of completeness. The results of this convergence analysis are reported in Table 7, where the last two columns are related to the errors of displacements and axial stresses in comparison with the 20B4-25L9 model. As evident from the reported values of this table, the classical and TE models of lower orders cannot accurately predict the displacements and axial stresses of the thin-walled beam structure with complex geometry.

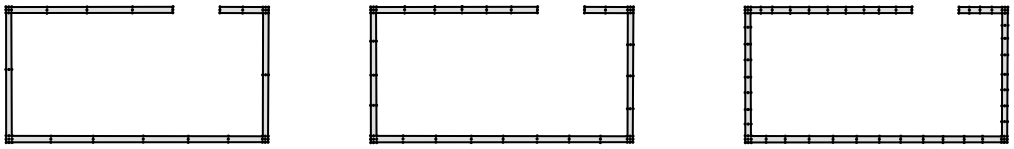

Figure 8: Discretization of the beam-3 cross-section based on different Lagrange expansions

Table 7: The convergence analysis of the vertical displacements at the bottom point (See point B of Fig. 4(c), $y = 10000mm$) and axial compressive stresses at the bottom point ($y = 1000mm$) of the beam 3- arbitrary cross-section- effect of the structural theory

Model	DOF	Displacement (mm)	Axial Stress (MPa)	Displacement Error %	Axial Stress Error %
20B4,TE=1	549	81.82	73.67	2.31	4.32
20B4,TE=2	1098	81.46	74.16	2.74	3.68
20B4,TE=5	3843	81.89	74.22	2.23	3.61
20B4,TE=10	12078	82.11	74.36	1.96	3.42
20B4,TE=15	24888	82.23	74.46	1.82	3.29
20B4-12L9	13725	83.66	76.93	0.11	0.09
20B4-16L9	18117	83.73	76.96	0.03	0.05
20B4-25L9	27999	83.76	77.00	0.00	0.00

5.1.4 Beam 4- Arbitrary cross-section

In order to investigate the effect of FE discretization, a convergence study is conducted for the displacements and stresses of the beam 4 with arbitrary cross-section. The beam is clamped at one end and subjected to a downward tip force $P = 90000N$ at the free end (point A in Fig. 4(d)). The results of the vertical displacements at the bottom point (See point B of Fig. 4(d), $y = 10000mm$) and axial compressive stresses at the bottom point ($y = 1000mm$) of the beam are reported in Table 8. The results of this table are presented for the beam elements with two nodes (B2), three nodes (B3), and four nodes (B4) elements, respectively. 17 Lagrange polynomials with nine nodes (17L9) are used for the expansion function over the cross-section. The last columns of table 8 are devoted to the error values of displacements and axial stresses compared to the 20B4-17L9 model.

Table 8: The convergence analysis of the vertical displacements at the bottom point (See point B of Fig. 4(d), $y = 10000mm$) and axial compressive stresses at the bottom point ($y = 1000mm$) of the beam 4- arbitrary cross-section- effect of FE discretization

Model	DOF	Displacement (mm)	Axial Stress (MPa)	Displacement Error %	Axial Stress Error %
5B2-17L9	1890	32.65	73.62	72.07	61.45
10B2-17L9	3465	65.79	104.78	43.72	45.13
20B2-17L9	6615	95.65	179.66	18.17	5.92
30B2-17L9	9765	105.88	181.07	9.42	5.18
50B2-17L9	16065	112.54	188.63	3.72	1.23
5B3-17L9	3465	114.78	140.19	1.81	26.59
10B3-17L9	6615	116.09	159.44	0.69	16.51
20B3-17L9	12915	116.65	187.21	0.21	1.97
30B3-17L9	19215	116.83	189.48	0.05	0.78
5B4-17L9	5040	116.02	153.45	0.75	19.65
10B4-17L9	9765	116.62	165.39	0.23	13.39
20B4-17L9	19215	116.90	190.98	0.00	0.00

In order to investigate the effect of structural theories, the same convergence study is conducted for the displacements and stresses of the beam 4 with arbitrary cross-section. Three LE models of

13L9, 17L9, and 26L9 are considered with 20B4 FE beams. As shown in Fig. 9, these LE models include 81, 105, and 159 Lagrange points, respectively. In addition, five TE models of order 1, 2, 5, 10, and 15 are considered for the sake of completeness. The results of this convergence analysis are reported in Table 9, where the last two columns are related to the errors of displacements and axial stresses in comparison with the 20B4-26L9 model.

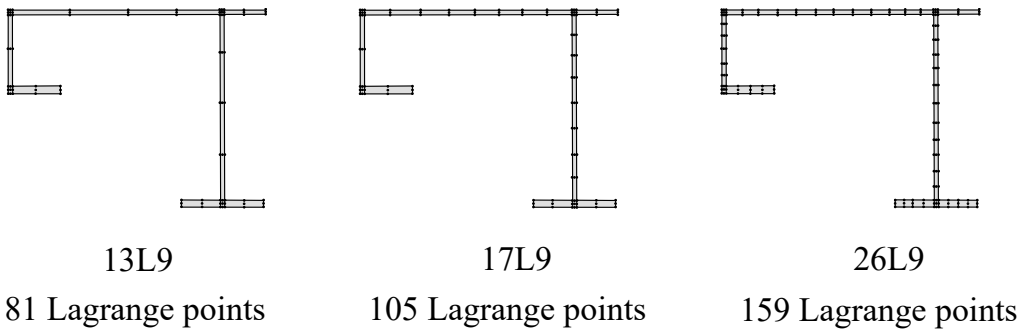

Figure 9: Discretization of the beam-4 cross-section based on different Lagrange expansions

Table 9: The convergence analysis of the vertical displacements at the bottom point (See point B of Fig. 4(d), $y = 10000mm$) and axial compressive stresses at the bottom point ($y = 1000mm$) of the beam 4- arbitrary cross-section- effect of the structural theory

Model	DOF	Displacement (mm)	Axial Stress (MPa)	Displacement Error %	Axial Stress Error %
20B4,TE=1	549	104.94	173.54	10.25	9.33
20B4,TE=2	1098	104.30	173.89	10.80	9.15
20B4,TE=5	3843	105.52	174.07	9.75	9.05
20B4,TE=10	12078	111.47	184.58	4.66	3.56
20B4,TE=15	24888	116.03	190.21	0.76	0.62
20B4-13L9	14823	116.87	190.82	0.05	0.30
20B4-17L9	19215	116.90	190.98	0.02	0.22
20B4-26L9	29097	116.93	191.41	0.00	0.00

5.2 Shear locking treatments

In this section, the results of displacements and axial stresses by some methods for the elimination of shear locking are investigated and compared. As introduced in Section 3.3 four methods of reduced, selective, full integration, and MITC are considered for the evaluation of shear locking in the beam elements.

5.2.1 Beam 1- C-shaped cross-section

For the first locking example, the C-shaped beam is considered. Fig. 10 plots the values of displacements based on the number of DOFs by using the different methods of full, selective, reduced integration, and MITC. As can be seen obviously in this figure, the locking significantly occurs for B2 linear beam elements by using the full integration. This phenomenon has been eliminated by using other locking-free methods of selective, reduced integration and MITC. in Table 10, the values of displacements and axial stresses are reported for B2, B3, and B4 elements respectively. The results are consistent with the prediction of the shear locking phenomenon in the linear elements with full integration. It should be noted that increasing the number of beam elements along the axis of the beam reduces the effect of shear locking considerably. This fact can be observed by the comparison of the evaluated displacements in Table 10 (also see Fig. 10a) for 5B2-14L9 and 14B2-14L9 models. Furthermore, it can be noted that the solutions of vertical displacements for the selective and MITC methods are similar.

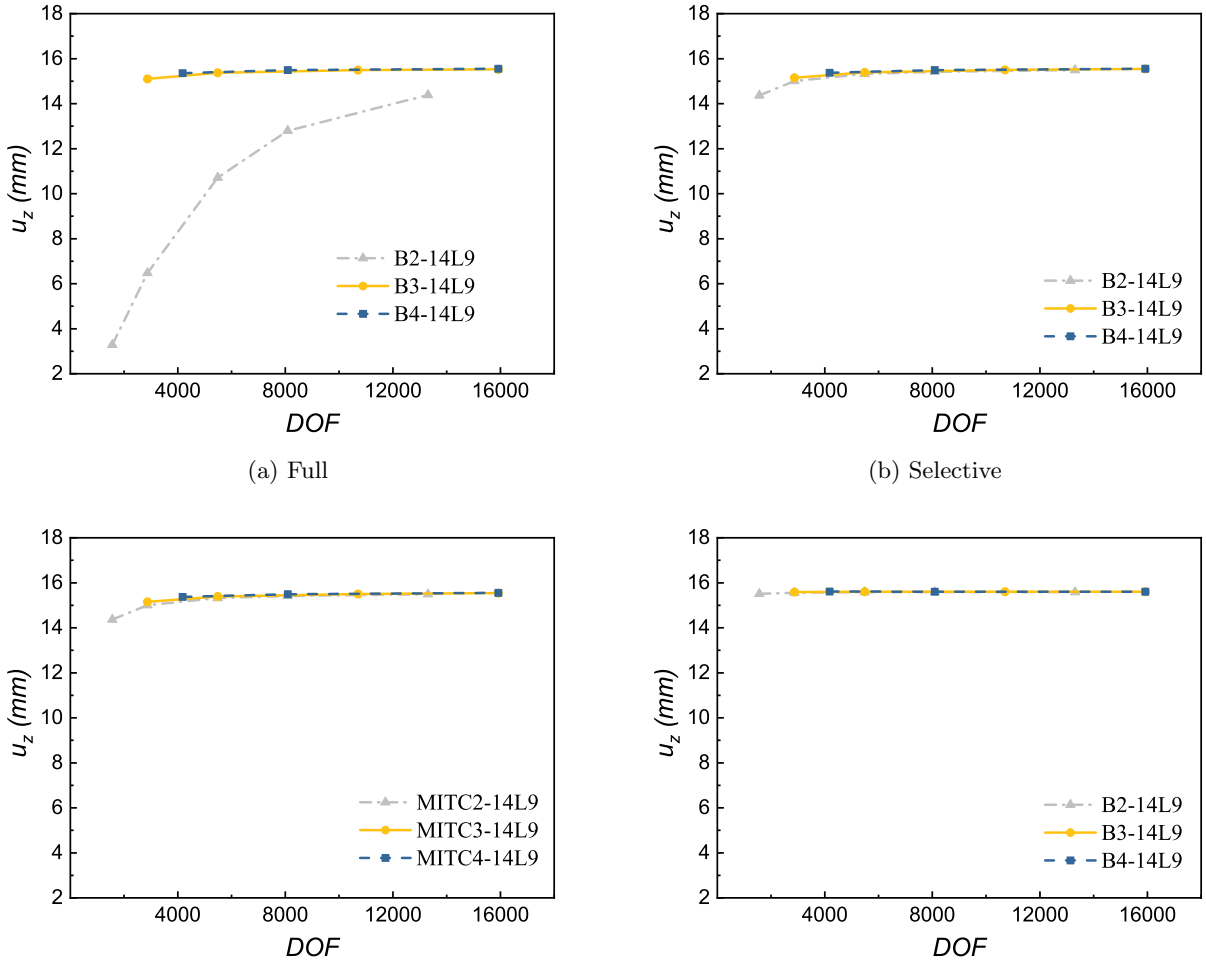

(a) Full

(b) Selective

(c) MITC

(d) Reduced

Figure 10: Evaluation of the effect of shear locking on the vertical displacements at the bottom point of the beam 1- C-shaped cross-section

Table 10: Evaluation of the effect of shear locking on the vertical displacements at the bottom point of the beam 1- C-shaped cross-section

		Displacement (mm)				Axial Stress (MPa)			
Models	DOF	Selective	Reduced	MITC	Full	Selective	Reduced	MITC	Full
5B2-14L9	1566	14.37	15.51	14.37	3.29	283.35	281.55	283.35	64.36
10B2-14L9	2871	15.01	15.56	15.01	6.48	202.21	114.11	202.21	87.13
20B2-14L9	5481	15.32	15.59	15.32	10.72	299.06	490.46	299.06	213.14
30B2-14L9	8091	15.42	15.59	15.42	12.80	293.77	70.74	293.77	235.51
50B2-14L9	13311	15.49	15.59	15.49	14.38	291.40	38.77	291.40	263.54
5B3-14L9	2871	15.15	15.59	15.15	15.10	240.84	182.36	240.84	139.42
10B3-14L9	5481	15.39	15.60	15.39	15.37	338.22	469.27	338.22	220.11
20B3-14L9	10701	15.50	15.60	15.50	15.49	272.85	492.40	272.85	272.46
30B3-14L9	15921	15.54	15.60	15.54	15.53	268.20	512.63	268.20	281.03
5B4-14L9	4176	15.37	15.61	15.37	15.36	274.14	277.32	274.14	187.63
10B4-14L9	8091	15.49	15.60	15.49	15.49	256.18	100.80	256.18	237.92
20B4-14L9	15921	15.55	15.60	15.55	15.55	263.82	496.75	263.82	283.48

5.2.2 Beam 2- T-shaped cross-section

For the second example of shear locking investigation, the T-shaped beam is considered. In Table 11, the values of displacements and axial stresses are reported for B2, B3, and B4 elements, respectively. The same comments as the previous example could be made about the results where the shear locking phenomenon occurs significantly in the linear elements with full integration method. The obtained results demonstrate the necessity of high order FE in order to overcome this issue. Use of the CUF results in models that are hardly influenced by shear locking. The shear locking effect should be carefully investigated while using the full integration method, especially for linear FE. It should be noted that the results of locking behavior for the other beams focused in this research paper are almost the same, and not presented here for the sake of brevity.

Table 11: Evaluation of the effect of shear locking on the vertical displacements at the bottom point of the beam 2- T-shaped cross-section

		Displacement (mm)				Axial Stress (MPa)			
Models	DOF	Selective	Reduced	MITC	Full	Selective	Reduced	MITC	Full
5B2-15L9	1674	23.94	25.14	57.10	10.84	496.93	493.63	496.93	228.88
10B2-15L9	3069	24.69	25.25	25.52	18.82	430.40	342.62	430.40	327.71
20B2-15L9	5859	25.04	25.30	8.19	23.20	494.21	671.25	494.21	474.24
30B2-15L9	8649	25.14	25.31	3.91	24.28	508.30	318.49	508.30	475.76
50B2-15L9	14229	25.22	25.31	1.46	24.90	495.95	331.88	495.95	486.85
5B3-15L9	3069	24.87	25.31	1.70	24.84	445.29	387.17	445.29	402.06
10B3-15L9	5859	25.11	25.32	0.67	25.10	509.26	629.58	509.26	441.04
20B3-15L9	11439	25.23	25.32	0.19	25.22	475.52	646.94	475.52	486.00
30B3-15L9	17019	25.26	25.32	0.03	25.26	485.29	644.23	485.29	489.21
5B4-15L9	4464	25.09	25.33	0.71	25.09	468.34	472.70	468.34	429.61
10B4-15L9	8649	25.22	25.32	0.19	25.22	507.72	377.02	507.72	467.26
20B4-15L9	17019	25.28	25.32	0.00	25.27	484.11	641.67	484.11	492.96

6 Higher-order modes detection via various models

In this section, the results of free vibration analysis and higher modes detection with cross-sectional deformation for the investigated beam structures of this paper are presented. First, for the purpose of validation of the proposed method, the free vibration modes and natural frequencies of a beam with cruciform cross-section are presented, and the results are compared with experiments and other available data from the literature as well as the Abaqus shell models. Then, the beam structures with C-shaped, T-shaped, and arbitrary cross-sections are analyzed based on their mode shapes and natural frequencies.

6.1 Validation case-cruciform beam

In order to validate the proposed method, a doubly clamped cruciform beam with a length of 670 mm is considered [31]. As indicated in schematic Fig. 11 (dimensions in millimeter), the cross-section of the beam is not geometrically symmetric. The isotropic material properties of Young's modulus ($E = 70\,GPa$), Poisson's ratio ($\nu = 0.3$), and density ($\rho = 2600\,Kg/m^3$) are considered for this beam model.

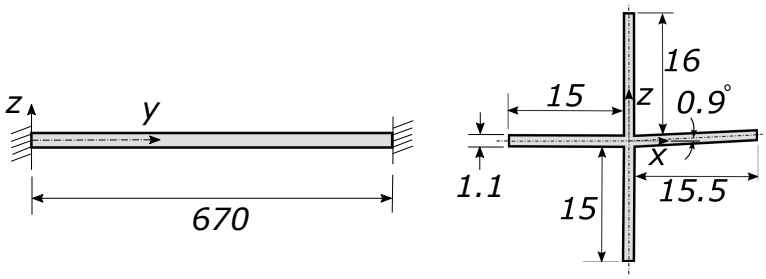

Figure 11: Schematic view of the cruciform beam

The details of the Abaqus shell and CUF-1D models used for the simulation of this cruciform beam are reported in Table 12. Moreover, the first ten natural frequencies of this beam are compared in Table 13 based on the used Abaqus shell and CUF-1D models. As shown in Fig. 12, the corresponding mode shapes 5 and 10 are also compared by using the CUF-1D and Abaqus shell models. It is observed from the contour plots of the mode shapes that the CUF-1D results with considerably lower computational costs correlate well with the more expensive Abaqus shell model. Moreover, in Table 14, the natural frequencies of the experimental method by Piana [31], and the other available literature for this case by Jrad [32] are compared with the proposed CUF-1D method. The results show that the proposed CUF method can predict the free vibration mode shapes and natural frequencies accurately and reliably.

Table 12: The details of Abaqus shell and CUF-1D models used for the simulation of the cruciform beam

Model	DOF	number of elements	Element type	Beam axis elements	Section discretization	Time (Sec)
Abaqus shell-coarse	6342	320	Quadratic S8R	40	9	25.16
Abaqus shell-medium	24198	1280	Quadratic S8R	80	17	31.47
Abaqus shell-fine	94470	5120	Quadratic S8R	120	33	53.89
CUF 1D-LE	2736	5B4	four nodes beam element	40	9L9	4.33
CUF 1D-LE	9765	10B4	four nodes beam element	80	17L9	11.48
CUF 1D-LE	27999	20B4	four nodes beam element	120	25L9	35.35

Table 13: The first ten natural frequencies of cruciform beam with doubly clamped edge conditions based on the used Abaqus shell and CUF-1D models

Modes	Abaqus shell-coarse	Abaqus shell-medium	Abaqus shell-fine	5B4-9L9	10B4-17L9	20B4-25L9
Mode 1	168.13	167.71	167.70	173.58	171.66	170.84
Mode 2	261.21	261.07	261.02	267.03	265.04	264.12
Mode 3	267.48	267.34	267.28	273.41	271.38	270.43
Mode 4	336.98	336.15	336.13	347.87	344.04	342.42
Mode 5	507.15	505.90	505.87	523.39	517.72	515.30
Mode 6	679.10	677.45	677.40	700.96	693.12	689.91
Mode 7	703.74	703.29	703.11	737.32	714.46	711.94
Mode 8	720.35	719.88	719.70	720.48	731.20	728.65
Mode 9	853.92	851.83	851.77	887.21	871.44	867.42
Mode 10	1031.8	1029.3	1029.2	1079.08	1052.84	1047.93

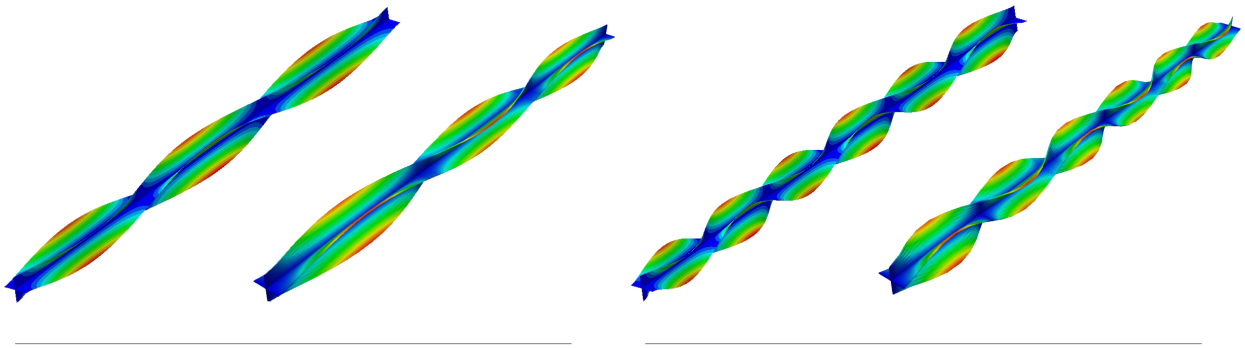

Figure 12: The comparison of free vibration mode shapes of Abaqus shell model and CUF 20B4-25L9

Table 14: The comparison of first ten natural frequencies of the cruciform beam with the available literature

Modes	Experimental results [31]	Numerical results[31]	B3Dw[32]	Abaqus-B31OS[32]	Abaqus shell-fine	CUF-1D 20B4-25L9	CUF-1D difference with experiments (%)
Mode 1	161.87	165.66	165.56	166.05	167.70	170.84	5.25
Mode 2	275.47	263.75	266.97	265.38	261.02	264.12	4.30
Mode 3	284.18	269.90	273.34	271.63	267.28	270.43	5.08
Mode 4	325.43	331.69	331.17	332.16	336.13	342.42	4.96
Mode 5	486.13	499.17	496.79	498.28	505.87	515.30	5.66
Mode 6	667.84	667.49	662.34	664.31	677.40	689.91	3.20
Mode 7	741.30	716.75	734.71	725.23	703.11	711.94	4.12
Mode 8	767.30	733.04	752.20	742.02	719.70	728.65	5.30
Mode 9	813.39	838.93	827.96	830.47	851.77	867.42	6.23
Mode 10	-	-	-	-	1029.2	1047.93	-

6.2 Beam 1- C-shaped cross-section

The first investigation of higher vibration modes with cross-sectional deformations is related to the C-shaped beam with clamped-free edge conditions. A full comparison of the natural frequencies based on the different structural theories of the proposed CUF-1D method is presented in Table 15, where the natural frequencies of B3Dw [32], BC2CM[19] methods, as well as Abaqus shell model, are compared. In Figs. 16, 17, and 18, the first 40 mode shapes of this beam are shown based on the TE=1, TE=10, and 22L9 models with 20B4 FE beams.

Table 15: Natural frequencies of beam 1 with clamped-free edge conditions based on different structural theories

Modes	20B4-22L9	20B4,TE=1	20B4,TE=2	20B4,TE=5	20B4,TE=10	20B4-8L9	20B4-14L9	Abaqus shell	B3Dw[32]	BC2CM[19]
Mode 1	25.10	33.59	33.84	33.63	26.39	25.12	25.11	25.00	25.37	25.37
Mode 2	33.57	73.00	73.33	53.09	33.57	33.58	33.57	33.51	33.58	33.63
Mode 3	96.19	208.23	209.15	110.72	96.56	96.32	96.22	96.07	98.16	98.15
Mode 4	135.58	435.55	436.06	203.13	141.18	137.72	136.05	134.61	148.43	148.41
Mode 5	151.31	573.27	480.15	206.62	160.67	152.83	151.63	150.51	209.84	210.14
Mode 6	156.40	624.08	573.55	419.71	169.17	158.10	156.72	155.20	410.02	409.97
Mode 7	166.95	650.22	1028.77	436.95	183.24	168.46	167.25	165.91	584.77	585.60
Mode 8	183.88	1097.31	1092.32	438.48	205.81	185.28	184.16	182.71	598.01	597.95
Mode 9	204.29	1139.50	1139.09	483.69	223.16	205.62	204.55	203.02	798.75	798.66
Mode 10	215.70	1762.99	1444.29	552.87	232.62	217.88	216.21	214.38	1025.78	1025.78
Mode 11	229.14	1872.25	1744.64	553.33	261.92	230.44	229.40	225.64	-	-
Mode 12	229.55	1950.34	2049.14	641.40	268.99	247.87	233.18	227.73	-	-
Mode 13	254.69	2055.96	2423.79	652.07	295.06	258.61	257.55	250.14	-	-
Mode 14	257.28	2549.61	2506.89	729.85	306.69	277.26	259.05	255.73	-	-
Mode 15	273.33	3249.50	3081.75	731.54	329.75	290.33	277.74	268.67	-	-
Mode 16	288.90	3115.53	3095.34	805.25	331.15	296.28	289.18	287.18	-	-
Mode 17	293.74	3120.41	3357.31	872.57	353.25	316.40	298.08	289.06	-	-
Mode 18	316.69	3437.52	3426.73	932.17	370.12	325.54	320.98	312.03	-	-
Mode 19	321.57	4266.07	4223.09	986.88	369.77	339.06	324.24	316.19	-	-
Mode 20	323.92	4409.07	4276.19	985.44	379.76	347.62	328.89	319.73	-	-
Mode 21	323.98	4368.58	4461.05	1027.46	383.12	352.11	327.49	322.03	-	-
Mode 22	344.40	4547.07	5119.94	1033.64	408.80	364.17	348.56	339.74	-	-
Mode 23	362.29	5449.09	5248.65	1076.31	411.87	366.25	362.66	360.20	-	-
Mode 24	374.97	5474.33	5390.34	1079.32	441.42	396.48	379.06	370.33	-	-
Mode 25	404.03	5616.75	5539.36	1121.52	456.46	406.26	404.47	401.74	-	-
Mode 26	409.21	5842.42	6258.72	1137.52	477.33	430.49	413.24	404.59	-	-
Mode 27	447.20	6544.88	6548.31	1164.09	503.81	451.81	449.66	442.62	-	-
Mode 28	449.12	6718.19	6690.49	1207.46	510.85	468.40	451.22	446.58	-	-
Mode 29	471.32	6864.92	7133.03	1216.18	516.69	500.86	484.71	464.38	-	-
Mode 30	488.90	7134.94	7299.74	1252.72	560.16	510.12	492.91	484.35	-	-
Mode 31	497.85	7686.00	7691.95	1265.32	554.52	524.70	498.53	495.07	-	-
Mode 32	534.25	7982.08	7904.82	1293.70	554.38	549.72	538.24	529.79	-	-
Mode 33	541.94	8113.12	8357.42	1304.41	585.74	553.70	544.43	539.89	-	-
Mode 34	549.83	8424.00	8849.89	1300.74	606.08	556.12	550.64	546.68	-	-
Mode 35	571.11	8864.03	9108.39	1338.04	608.12	581.46	578.92	558.61	-	-
Mode 36	578.16	9253.18	9141.08	1352.34	655.86	605.70	588.19	576.65	-	-
Mode 37	584.20	9361.35	9431.04	1372.11	660.99	610.00	601.73	580.09	-	-
Mode 38	600.87	9709.00	10025.34	1407.62	665.29	659.25	606.98	587.46	-	-
Mode 39	606.06	10072.19	10382.11	1408.09	705.34	670.05	636.62	602.08	-	-
Mode 40	621.98	10517.44	10509.69	1445.67	709.34	716.91	641.26	608.10	-	-

Table 16: First 40 mode shapes of beam 1, 20B4,TE=1 model with clamped-free edge conditions

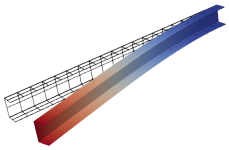 Mode l	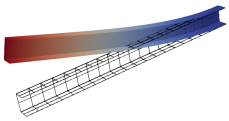 Mode 2	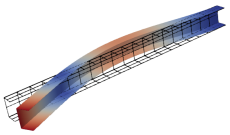 Mode 3	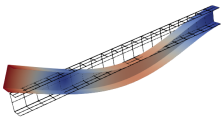 Mode 4	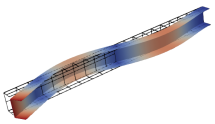 Mode 5
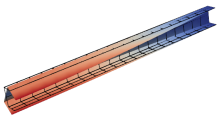 Mode 6	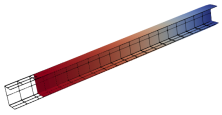 Mode 7	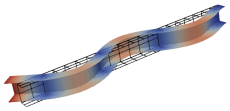 Mode 8	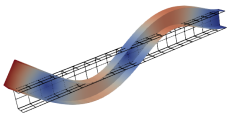 Mode 9	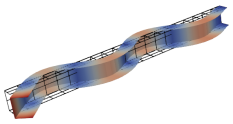 Mode 10
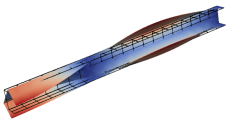 Mode 1l	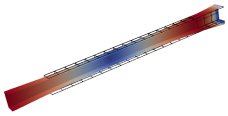 Mode 12	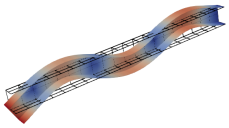 Mode 13	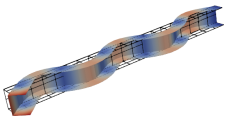 Mode 14	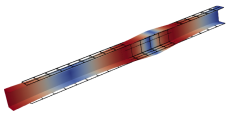 Mode 15
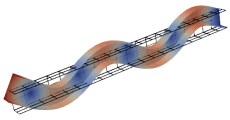 Mode 16	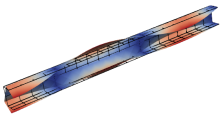 Mode 17	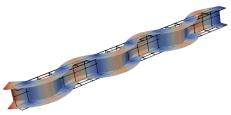 Mode 18	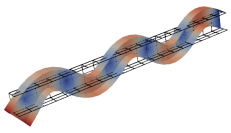 Mode 19	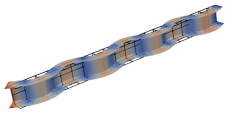 Mode 20
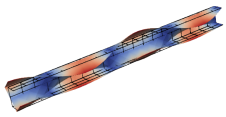 Mode 2l	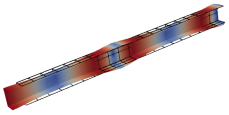 Mode 22	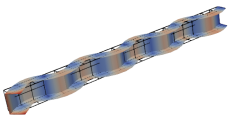 Mode 23	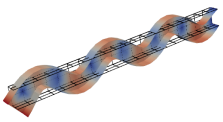 Mode 24	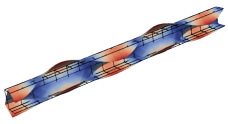 Mode 25
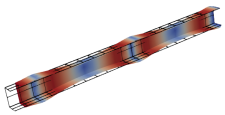 Mode 26	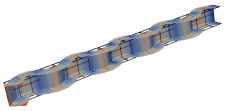 Mode 27	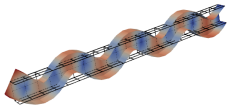 Mode 28	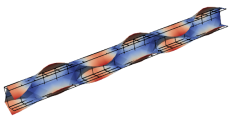 Mode 29	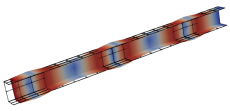 Mode 30
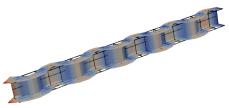 Mode 3l	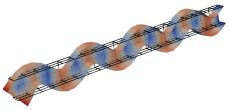 Mode 32	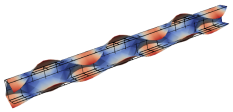 Mode 33	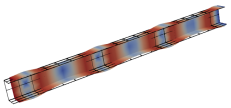 Mode 34	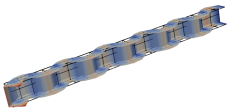 Mode 35
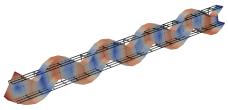 Mode 36	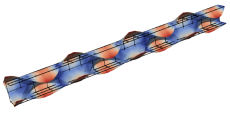 Mode 37	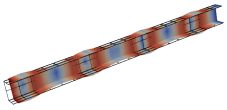 Mode 38	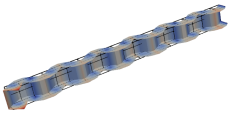 Mode 39	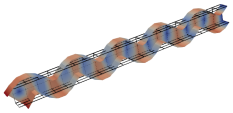 Mode 40

Table 17: First 40 mode shapes of beam 1, 20B4,TE=10 model with clamped-free edge conditions

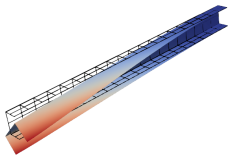 Mode 1	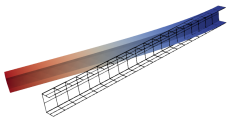 Mode 2	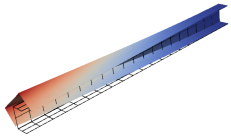 Mode 3	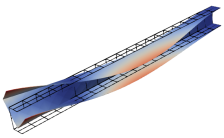 Mode 4	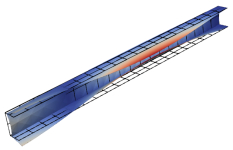 Mode 5
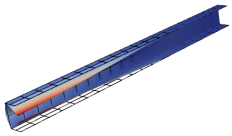 Mode 6	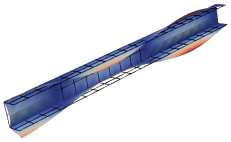 Mode 7	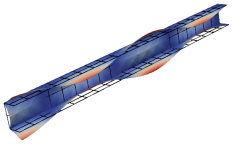 Mode 8	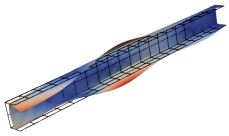 Mode 9	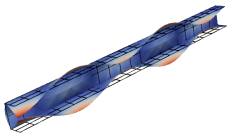 Mode 10
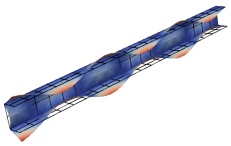 Mode 11	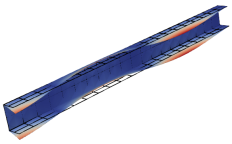 Mode 12	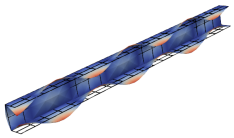 Mode 13	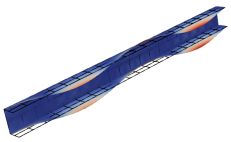 Mode 14	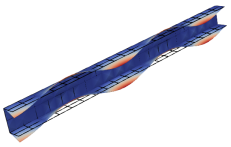 Mode 15
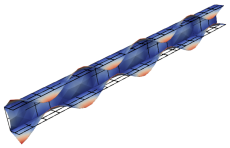 Mode 16	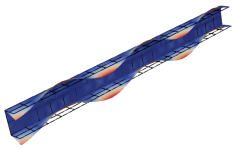 Mode 17	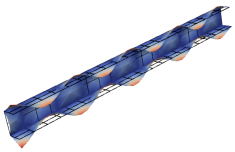 Mode 18	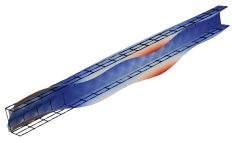 Mode 19	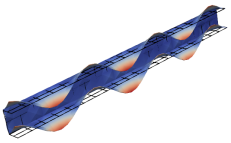 Mode 20
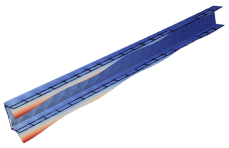 Mode 21	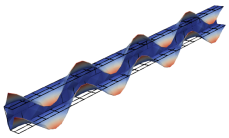 Mode 22	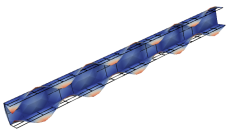 Mode 23	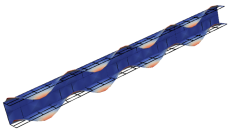 Mode 24	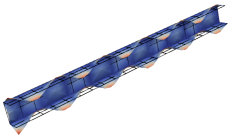 Mode 25
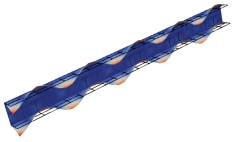 Mode 26	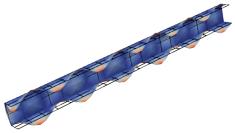 Mode 27	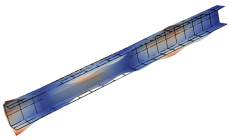 Mode 28	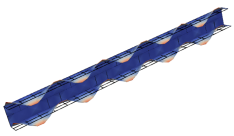 Mode 29	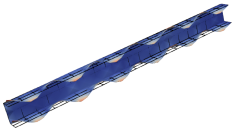 Mode 30
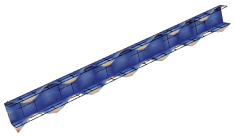 Mode 31	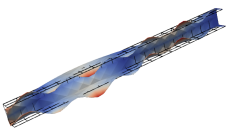 Mode 32	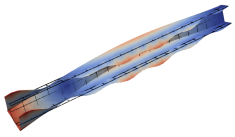 Mode 33	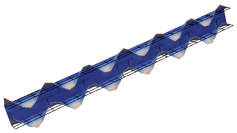 Mode 34	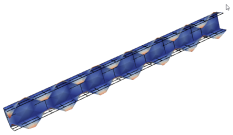 Mode 35
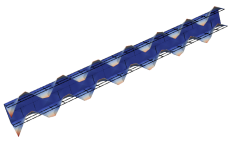 Mode 36	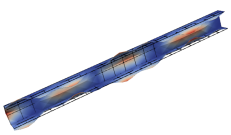 Mode 37	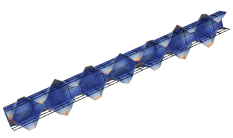 Mode 38	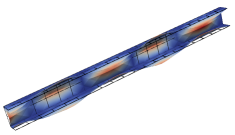 Mode 39	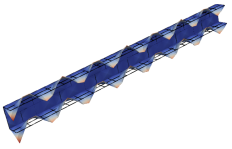 Mode 40

Table 18: First 40 mode shapes of beam 1, 20B4-22L9 model with clamped-free edge conditions

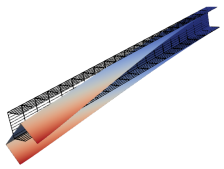 Mode l	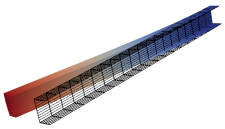 Mode 2	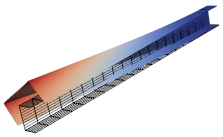 Mode 3	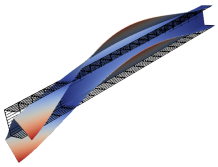 Mode 4	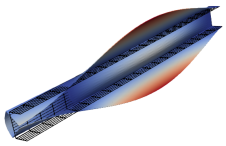 Mode 5
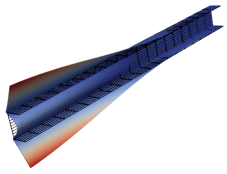 Mode 6	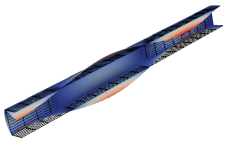 Mode 7	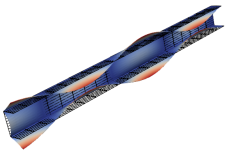 Mode 8	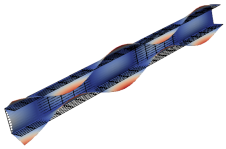 Mode 9	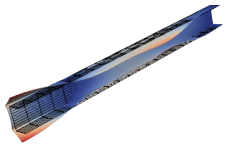 Mode 10
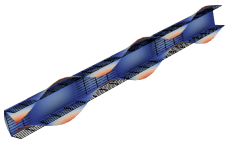 Mode 11	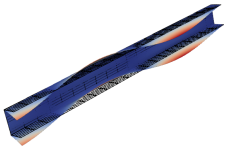 Mode 12	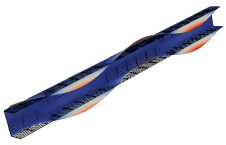 Mode 13	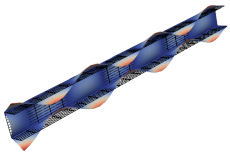 Mode 14	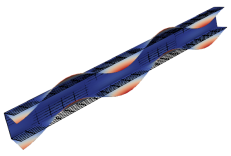 Mode 15
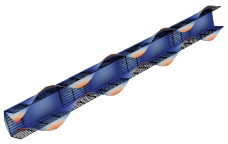 Mode 16	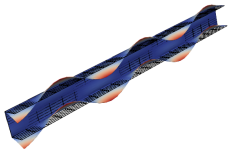 Mode 17	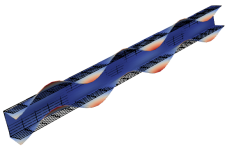 Mode 18	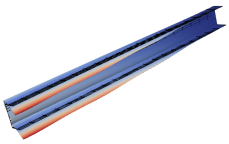 Mode 19	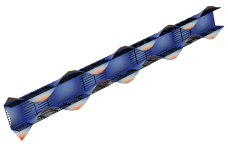 Mode 20
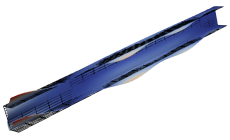 Mode 2l	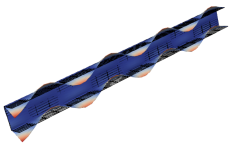 Mode 22	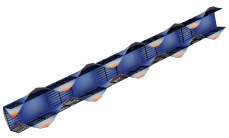 Mode 23	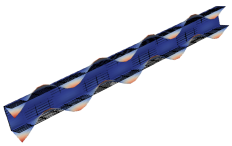 Mode 24	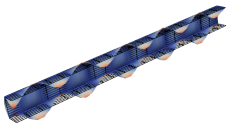 Mode 25
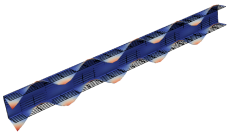 Mode 26	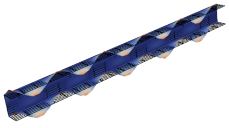 Mode 27	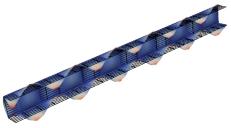 Mode 28	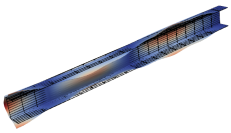 Mode 29	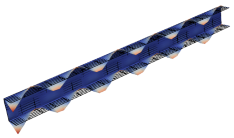 Mode 30
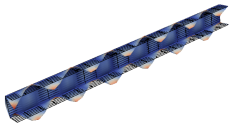 Mode 3l	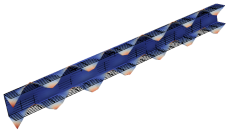 Mode 32	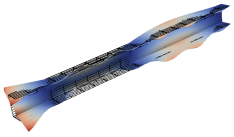 Mode 33	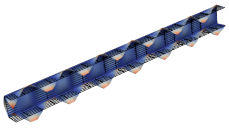 Mode 34	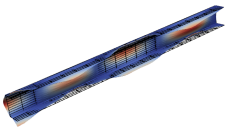 Mode 35
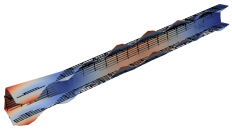 Mode 36	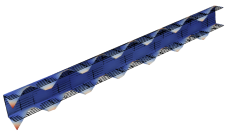 Mode 37	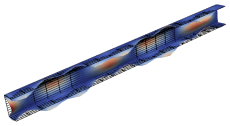 Mode 38	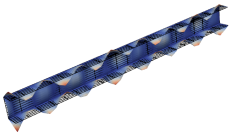 Mode 39	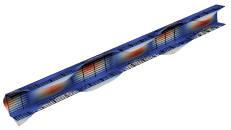 Mode 40

For the sake of completeness, a shell model is used for the free vibration analysis of the structure. The details of the Abaqus shell model used for the simulation of the C-shaped beam are reported in Table 19. As shown in Fig. 13, for the corresponding modes number 40, the contour plots of mode shapes and the natural frequencies are compared by using the CUF-1D and Abaqus shell models. It is observed from the contour plots of the mode shapes that the CUF-1D results with considerably lower computational costs correlate well with the more expensive Abaqus shell model.

Table 19: The details of Abaqus shell model used for the simulation of beam 1. CUF DOF = 17019.

Model	DOF	number of elements	Element type	Beam axis elements	Cross-Section discretization
Shell	12738	660	Quadratic S8R	60	8

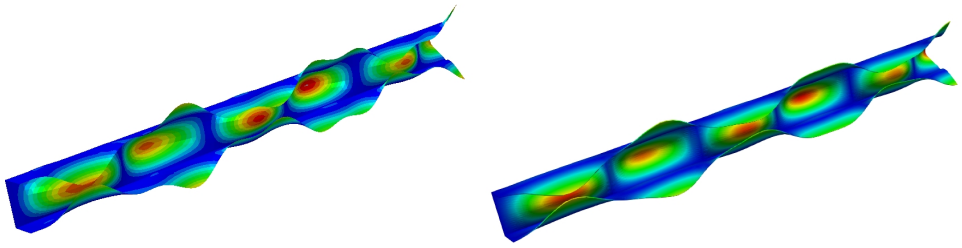

(a) Abaqus shell, Mode 40, Freq=608.10 Hz (b) CUF 1D, Mode 40, Freq=621.97 Hz

Figure 13: The comparison of free vibration mode shapes of Abaqus shell model and CUF 20B4-22L9

Some comments could be made according to the results of Figs. 16, 17, 18, and Table 15 of the natural frequencies.

1. Classical beam theories and the linear TE of order one are not capable of capturing many cross-sectional deformations related to the bending or torsion; instead, they show rigid-cross section modes that do not really exist.

2. In contradiction with the TE=1 model, the other structural models of TE=10 and 22L9 share some common modes

3. The need for the models capable of detecting cross-sectional deformations is outlined.

4. The values of natural frequencies obtained by the CUF-1D (with considerably lower computational costs) correlate reasonably well with the more expensive Abaqus shell model

5. It can be observed in the contour plots of the mode shapes that many of them are not corresponding to each other. Therefore, the use of MAC analysis is necessary to investigate the corresponding modes related to each theory.

The MAC is defined as a scalar that represents the degree of consistency between two distinct modal vectors in such a way that the values change from 0 to 1. The MAC value of 0 represents no consistent correspondence of the models. The MAC is obtained according to the following equation [49, 68, 69, 70]:

$$MAC_{ij} = \frac{\left|\{\varphi_{A_i}\}^T \{\varphi_{B_j}\}\right|^2}{\{\varphi_{A_i}\}^T \{\varphi_{A_i}\} \{\varphi_{B_j}\} \{\varphi_{B_j}\}^T} \tag{18}$$

where φ_{A_i} is the i th eigenvector of model A, and φ_{B_j} is the j th eigenvector of model B. In the following, by using the MAC analysis (see Fig. 14), a comparison of the corresponding natural frequencies based on the different structural theories of the proposed CUF-1D method is presented

in Table 20, where the natural frequencies of B3Dw [32], BC2CM[19] methods, as well as Abaqus shell model, are also compared. It should be noted that the differences between the reference and the proposed solutions is that the reference uses analytical approaches. It adopted elements with 2 nodes and 7 DOFs per node in order to consider the effects of bending and torsional couplings. It should be considered that it is difficult to make a one by one comparison between the present approach and the reference one, because the latter could be seen as a combination of low order theories, which are here described as TE1 and TE2.

Table 20: Natural frequencies of beam 1 with clamped-free edge conditions based on different structural theories for the corresponding mode shapes using MAC (see Table 15 for comparison)

Modes	20B4-22L9	20B4,TE=1	20B4,TE=2	20B4,TE=5	20B4,TE=10	20B4-8L9	20B4-14L9	Abaqus shell	B3Dw[32]	BC2CM[19]
Mode 1	25.10	-	-	-	26.39	25.12	25.11	25.00	25.37	25.37
Mode 2	33.57	33.59	33.84	33.63	33.57	33.58	33.57	33.51	33.58	33.63
Mode 3	96.19	-	-	110.72	96.56	96.32	96.22	96.07	98.16	98.15
Mode 4	135.58	-	-	206.62	141.18	137.72	136.05	134.61	148.43	148.41
Mode 5	151.31	-	-	-	160.67	152.83	151.63	150.51	209.84	210.14
Mode 6	156.40	-	-	-	169.17	158.10	156.72	155.20	410.02	409.97
Mode 7	166.95	-	-	-	183.24	168.46	167.25	165.91	584.77	585.60
Mode 8	183.88	-	-	-	205.81	185.28	184.16	182.71	598.01	597.95
Mode 9	204.29	-	-	-	-	205.62	204.55	203.02	798.75	798.66
Mode 10	215.70	-	-	-	223.16	217.88	216.21	214.38	1025.78	1025.78
Mode 11	229.14	-	-	731.54	261.92	230.44	229.40	225.64	-	-
Mode 12	229.55	-	-	-	268.99	247.87	233.18	227.73	-	-
Mode 13	254.69	-	-	-	306.69	277.26	259.05	250.14	-	-
Mode 14	257.28	-	-	805.25	295.06	258.61	257.55	255.73	-	-
Mode 15	273.33	-	-	-	329.75	296.28	277.74	268.67	-	-
Mode 16	288.90	-	-	872.57	331.15	290.33	289.18	287.18	-	-
Mode 17	293.74	-	-	-	353.25	316.40	298.08	289.06	-	-
Mode 18	316.69	-	-	-	-	339.06	320.98	312.03	-	-
Mode 19	321.57	-	-	-	383.12	352.11	327.49	316.19	-	-
Mode 20	323.92	-	-	932.17	370.12	325.54	324.24	319.73	-	-
Mode 21	323.98	-	-	-	-	347.62	328.89	322.03	-	-
Mode 22	344.40	-	-	1265.32	408.80	366.25	348.56	339.74	-	-
Mode 23	362.29	-	-	985.44	411.87	364.17	362.66	360.20	-	-
Mode 24	374.97	-	-	-	441.42	396.48	379.06	370.33	-	-
Mode 25	404.03	-	-	1033.64	456.46	406.26	404.47	401.74	-	-
Mode 26	409.21	-	-	1338.04	477.33	430.49	413.24	404.59	-	-
Mode 27	447.20	-	-	1372.11	516.69	468.40	451.22	442.62	-	-
Mode 28	449.12	-	-	-	503.81	451.81	449.66	446.58	-	-
Mode 29	471.32	-	-	-	510.85	524.70	484.71	464.38	-	-
Mode 30	488.90	-	-	1407.62	-	510.12	492.91	484.35	-	-
Mode 31	497.85	-	-	1121.52	554.52	500.86	498.53	495.07	-	-
Mode 32	534.25	-	-	1445.67	606.08	-	538.24	529.79	-	-
Mode 33	541.94	-	-	-	554.38	549.72	544.43	539.89	-	-
Mode 34	549.83	-	-	1164.09	608.12	553.70	550.64	546.68	-	-
Mode 35	571.11	-	-	-	660.99	-	601.73	558.61	-	-
Mode 36	578.16	-	-	-	585.74	581.46	578.92	576.65	-	-
Mode 37	584.20	-	-	-	655.86	605.70	588.19	580.09	-	-
Mode 38	600.87	-	-	-	705.34	-	636.62	587.46	-	-
Mode 39	606.06	-	-	-	-	610.00	-	602.08	-	-
Mode 40	621.98	-	-	-	-	-	-	608.10	-	-

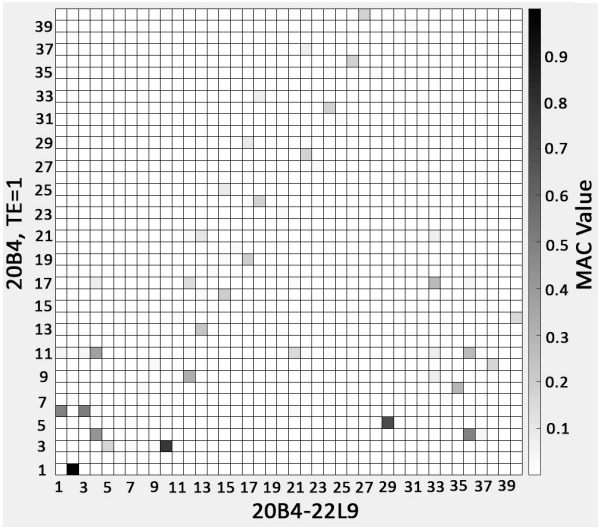

(a) 20B4,TE=1

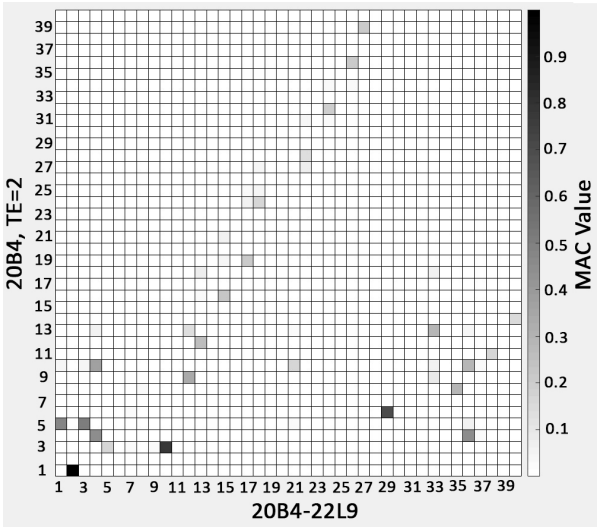

(b) 20B4,TE=2

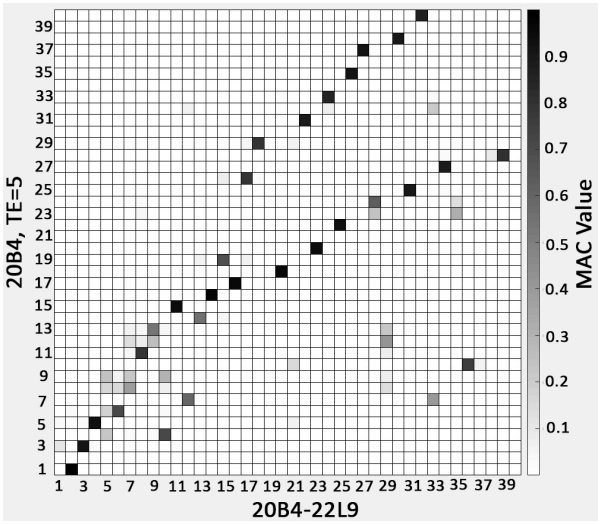

(c) 20B4,TE=5

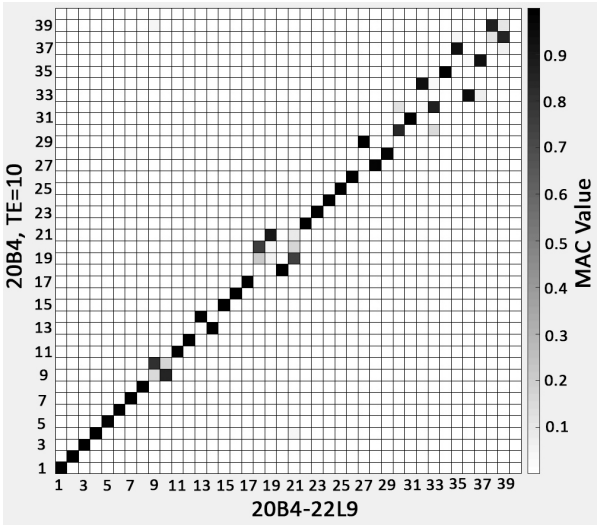

(d) 20B4,TE=10

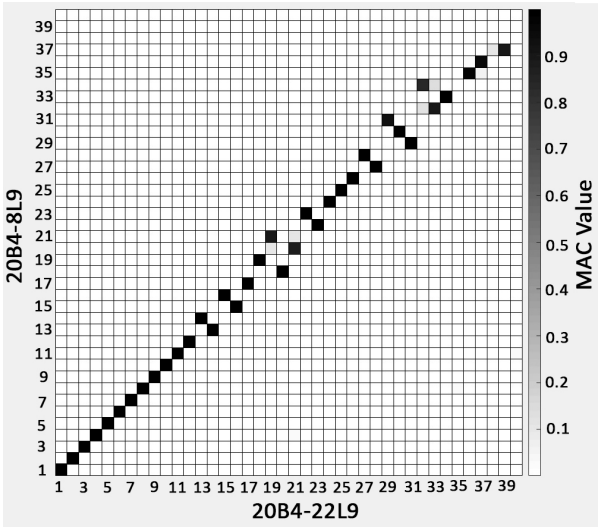

(e) 20B4-8L9

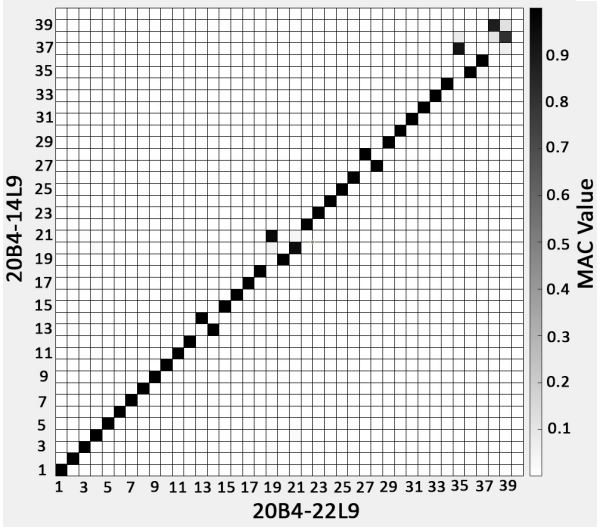

(f) 20B4-14L9

Figure 14: The comparison of free vibration modes using MAC for beam 1 with clamped-free edge conditions based on different structural theories and 20B4-22L9 model

6.3 Beam 2- T-shaped cross-section

The second investigation of higher vibration modes with cross-sectional deformations is related to the T-shaped beam with clamped-free edge conditions. The first 40 mode shapes of this beam are shown in Fig. 23 based on the 20B4-23L9 model. The details of the Abaqus shell model used for the simulation of the T-shaped beam are reported in Table 21. By using the MAC analysis, a comparison of the corresponding natural frequencies based on the different structural theories of the proposed CUF-1D method is presented in Table 22, where the natural frequencies of B3Dw [32], BC2CM[19] methods, as well as Abaqus shell model, are also compared.

Table 21: The details of Abaqus shell model used for the simulation of beam 2. CUF DOF = 25803.

Model	DOF	number of elements	Element type	Beam axis elements	Cross-Section discretization
Shell	24198	1280	Quadratic S8R	80	16

Table 22: Natural frequencies of beam 2 with clamped-free edge conditions based on different structural theories for the corresponding mode shapes using MAC

Modes	20B4-23L9	20B4,TE=1	20B4,TE=2	20B4,TE=5	20B4,TE=10	20B4-9L9	20B4-15L9	Abaqus shell	B3Dw[32]	BC2CM[19]
Mode 1	12.54	-	-	-	12.93	12.57	12.55	12.43	12.48	12.48
Mode 2	27.50	-	-	48.28	30.33	27.71	27.59	27.09	27.62	27.62
Mode 3	45.42	-	-	-	45.43	45.42	45.42	45.27	45.75	45.75
Mode 4	54.68	-	-	-	60.23	55.14	54.89	53.99	55.90	55.90
Mode 5	88.32	-	-	-	96.35	89.01	88.61	87.18	92.66	92.68
Mode 6	124.21	-	-	-	130.59	124.84	124.48	122.58	128.84	128.84
Mode 7	130.74	-	-	-	141.13	131.57	131.07	128.97	141.80	141.83
Mode 8	166.59	-	-	240.45	179.65	167.87	167.07	164.26	188.27	188.31
Mode 9	205.85	-	-	279.77	219.39	207.32	206.37	203.12	236.87	236.95
Mode 10	250.20	-	-	-	264.02	251.83	250.75	247.08	282.85	282.85
Mode 11	263.02	272.56	271.49	264.22	263.46	263.17	263.06	261.84	-	-
Mode 12	298.44	-	-	-	-	300.11	298.98	295.04	-	-
Mode 13	315.93	-	-	-	319.22	316.37	316.05	312.55	-	-
Mode 14	354.59	-	-	427.15	368.44	356.52	355.19	350.82	-	-
Mode 15	415.57	-	-	486.95	429.36	417.65	416.19	411.51	-	-
Mode 16	459.32	-	-	-	478.93	462.10	460.11	453.70	-	-
Mode 17	482.26	-	-	-	496.67	484.66	482.98	477.57	-	-
Mode 18	487.54	-	-	-	511.15	490.55	488.48	482.23	-	-
Mode 19	525.06	-	-	-	541.66	528.18	526.05	520.31	-	-
Mode 20	553.70	-	-	-	-	556.73	554.69	548.26	-	-
Mode 21	560.24	-	-	-	-	563.11	561.13	555.21	-	-
Mode 22	628.34	-	-	-	662.19	632.78	629.89	622.36	-	-
Mode 23	639.20	-	-	705.85	-	641.79	639.93	634.02	-	-
Mode 24	649.55	-	-	649.66	649.58	649.57	649.55	649.13	-	-
Mode 25	662.35	715.18	769.26	670.59	665.68	663.84	662.69	658.32	-	-
Mode 26	677.64	-	-	-	717.97	682.37	679.44	669.76	-	-
Mode 27	725.15	-	-	-	-	728.39	726.15	719.34	-	-
Mode 28	732.66	-	-	-	779.94	739.58	734.87	726.48	-	-
Mode 29	816.96	-	-	-	-	-	819.10	809.46	-	-
Mode 30	823.29	-	-	-	-	-	824.91	816.58	-	-
Mode 31	902.95	-	-	-	963.75	913.63	906.19	893.08	-	-
Mode 32	923.70	-	-	-	935.53	927.05	924.58	916.21	-	-
Mode 33	965.36	-	-	-	1006.02	972.81	967.76	945.81	-	-
Mode 34	994.64	-	-	1363.44	1063.81	1007.73	998.38	982.57	-	-
Mode 35	1032.09	-	-	1096.39	1044.03	1035.54	1033.00	1022.73	-	-
Mode 36	1084.75	-	-	-	-	1099.84	1088.86	1060.54	-	-
Mode 37	1107.53	-	-	-	1263.43	1140.75	1115.41	1070.11	-	-
Mode 38	1120.25	-	-	-	-	-	1128.13	1073.57	-	-
Mode 39	1140.14	1294.36	1269.53	1171.98	1153.91	1147.42	1141.59	1097.15	-	-
Mode 40	1142.58	-	-	-	-	-	1147.82	1130.12	-	-

Table 23: First 40 mode shapes of beam 2, 20B4-23L9 model with clamped-free edge conditions

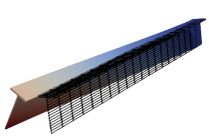 Mode 1	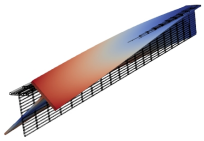 Mode 2	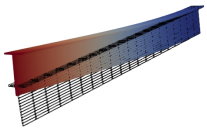 Mode 3	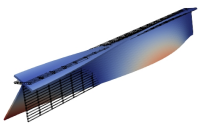 Mode 4	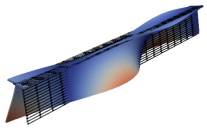 Mode 5
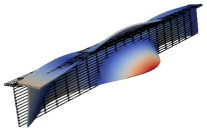 Mode 6	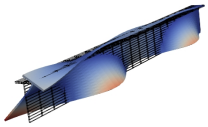 Mode 7	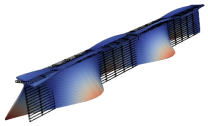 Mode 8	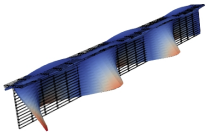 Mode 9	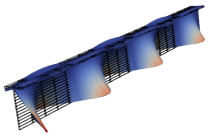 Mode 10
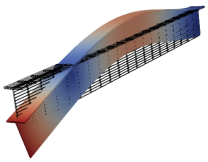 Mode 11	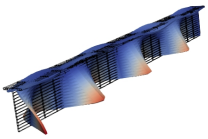 Mode 12	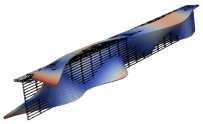 Mode 13	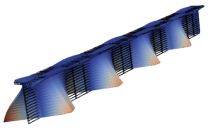 Mode 14	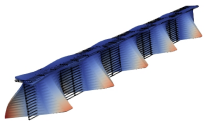 Mode 15
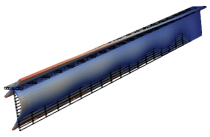 Mode 16	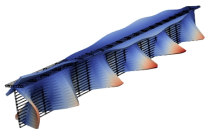 Mode 17	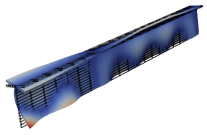 Mode 18	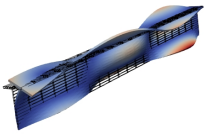 Mode 19	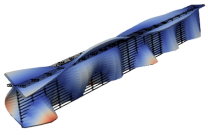 Mode 20
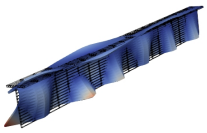 Mode 21	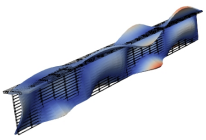 Mode 22	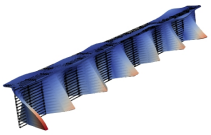 Mode 23	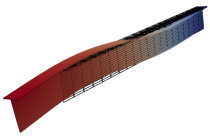 Mode 24	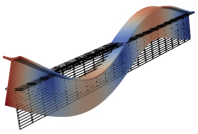 Mode 25
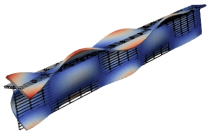 Mode 26	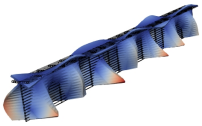 Mode 27	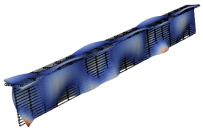 Mode 28	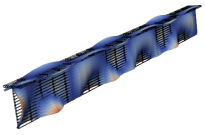 Mode 29	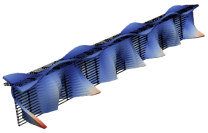 Mode 30
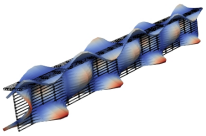 Mode 31	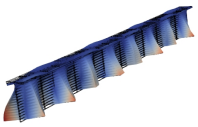 Mode 32	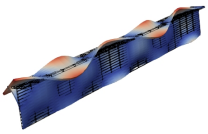 Mode 33	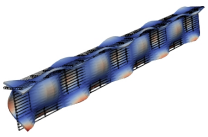 Mode 34	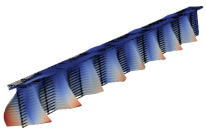 Mode 35
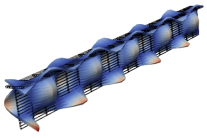 Mode 36	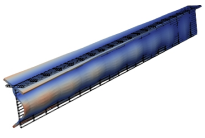 Mode 37	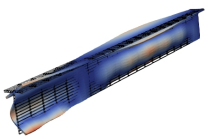 Mode 38	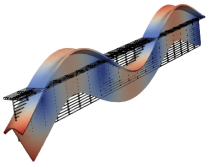 Mode 39	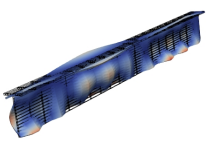 Mode 40

6.4 Beam 3- Arbitrary cross-section

The third investigation of higher vibration modes with cross-sectional deformations is related to the beam 3 (arbitrary cross-section) with clamped-free edge conditions. The first 40 mode shapes of this beam are shown in Fig. 26 based on the 20B4-25L9 model. The details of the Abaqus shell model used for the simulation of the beam 3 are reported in Table 24. By using the MAC analysis, a comparison of the corresponding natural frequencies based on the different structural theories of the proposed CUF-1D method is presented in Table 25, where the natural frequencies of B3Dw [32], BC2CM[19] methods, as well as Abaqus shell model, are also compared.

Table 24: The details of Abaqus shell model used for the simulation of beam 3. CUF DOF = 27999.

Model	DOF	number of elements	Element type	Beam axis elements	Cross-Section discretization
Shell	64854	3520	Quadratic S8R	80	42

Table 25: Natural frequencies of beam 3 with clamped-free edge conditions based on different structural theories for the corresponding mode shapes using MAC

Modes	20B4-25L9	20B4,TE=1	20B4,TE=2	20B4,TE=5	20B4,TE=10	20B4-12L9	20B4-16L9	Abaqus shell	B3Dw[32]	BC2CM[19]
Mode 1	3.27	-	-	-	-	3.27	3.27	3.26	3.27	3.27
Mode 2	4.80	-	-	-	-	4.81	4.80	4.79	4.82	4.82
Mode 3	12.37	-	-	-	-	12.38	12.38	12.35	12.63	12.63
Mode 4	18.44	-	-	-	-	18.46	18.45	18.35	19.17	19.17
Mode 5	25.50	-	-	-	-	25.58	25.53	25.35	28.85	28.85
Mode 6	37.73	-	-	-	-	38.28	37.91	37.07	52.71	52.71
Mode 7	38.20	-	-	-	-	-	38.29	37.77	73.68	73.68
Mode 8	44.01	-	-	-	-	44.49	44.17	43.43	79.77	79.77
Mode 9	55.53	-	-	-	-	55.86	55.62	55.08	102.56	102.56
Mode 10	56.23	-	-	-	-	56.92	56.43	55.66	128.07	128.10
Mode 11	67.58	-	-	-	-	68.11	67.74	67.12	154.80	154.81
Mode 12	73.55	-	-	-	-	-	74.24	72.05	168.52	168.55
Mode 13	74.30	-	-	-	-	-	74.95	72.67	197.56	197.56
Mode 14	75.29	-	-	-	-	78.52	76.18	73.46	250.16	-
Mode 15	78.71	-	-	-	-	81.64	79.50	77.07	-	-
Mode 16	82.26	-	-	-	-	85.03	83.04	80.44	-	-
Mode 17	85.97	-	-	-	-	90.98	87.10	83.80	-	-
Mode 18	93.85	-	-	-	-	96.38	94.59	92.02	-	-
Mode 19	95.43	-	-	-	-	101.66	96.80	92.94	-	-
Mode 20	97.63	-	-	-	-	99.26	97.99	96.88	-	-
Mode 21	103.70	-	-	-	-	104.41	103.97	101.29	-	-
Mode 22	104.05	-	-	-	-	-	105.55	103.09	-	-
Mode 23	111.89	-	-	-	-	114.79	112.73	109.69	-	-
Mode 24	112.91	-	-	-	-	-	114.48	110.31	-	-
Mode 25	122.04	-	-	-	-	129.91	123.74	119.05	-	-
Mode 26	128.22	-	-	-	-	128.23	128.22	128.15	-	-
Mode 27	131.93	-	-	-	-	140.08	133.69	128.83	-	-
Mode 28	133.94	-	-	-	-	142.57	-	130.61	-	-
Mode 29	135.02	-	-	-	-	138.64	-	132.79	-	-
Mode 30	142.84	-	-	-	-	151.09	144.64	139.66	-	-
Mode 31	148.90	-	-	-	-	167.84	152.89	143.39	-	-
Mode 32	152.58	-	-	-	-	-	156.50	147.27	-	-
Mode 33	154.03	-	-	-	-	-	-	150.53	-	-
Mode 34	155.96	-	-	-	-	-	-	152.23	-	-
Mode 35	157.38	-	-	-	-	-	-	155.05	-	-
Mode 36	161.28	-	-	-	-	165.78	162.53	158.64	-	-
Mode 37	166.97	-	-	-	-	175.53	168.84	163.60	-	-
Mode 38	169.74	-	-	-	-	-	170.33	168.55	-	-
Mode 39	180.35	-	-	-	-	188.96	182.28	176.84	-	-
Mode 40	186.40	-	-	-	-	-	188.28	183.35	-	-

Table 26: First 40 mode shapes of beam 3, 20B4-25L9 model with clamped-free edge conditions

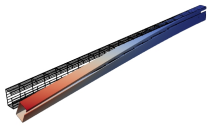 Mode 1	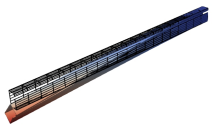 Mode 2	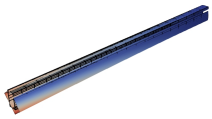 Mode 3	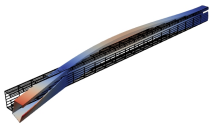 Mode 4	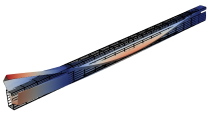 Mode 5
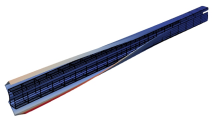 Mode 6	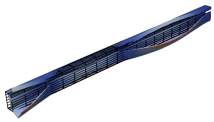 Mode 7	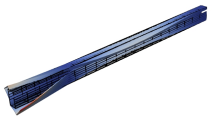 Mode 8	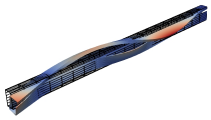 Mode 9	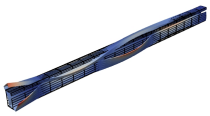 Mode 10
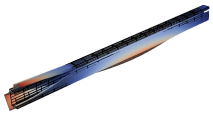 Mode 11	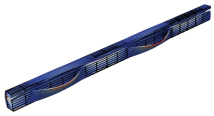 Mode 12	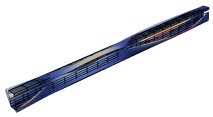 Mode 13	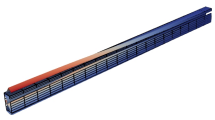 Mode 14	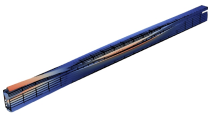 Mode 15
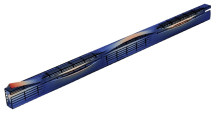 Mode 16	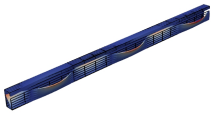 Mode 17	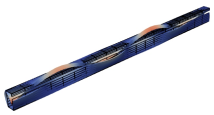 Mode 18	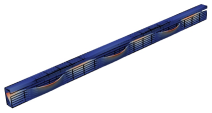 Mode 19	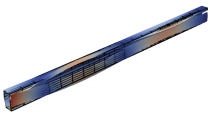 Mode 20
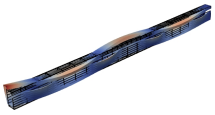 Mode 21	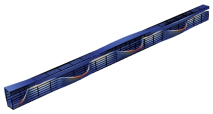 Mode 22	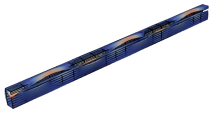 Mode 23	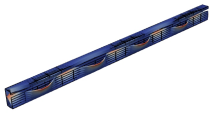 Mode 24	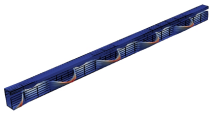 Mode 25
 Mode 26	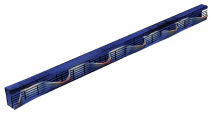 Mode 27	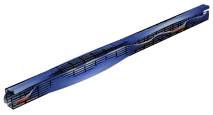 Mode 28	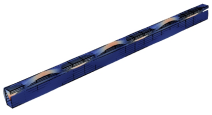 Mode 29	 Mode 30
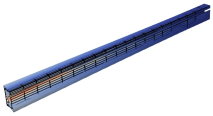 Mode 31	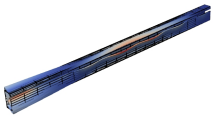 Mode 32	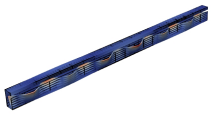 Mode 33	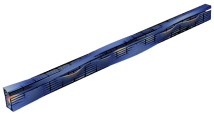 Mode 34	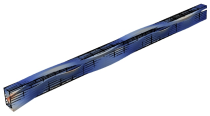 Mode 35
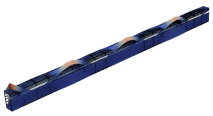 Mode 36	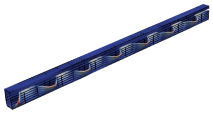 Mode 37	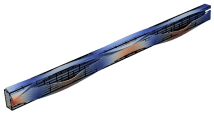 Mode 38	 Mode 39	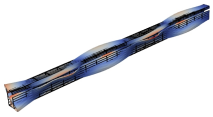 Mode 40

6.5 Beam 4- Arbitrary cross-section

The last investigation of higher vibration modes with cross-sectional deformations is related to the beam 4 (arbitrary cross-section) with clamped-free edge conditions. The first 40 mode shapes of this beam are shown in Fig. 27 based on the 20B4-26L9 model. The details of the Abaqus shell model used for the simulation of the beam 4 are reported in Table 28. By using the MAC analysis, a comparison of the corresponding natural frequencies based on the different structural theories of

the proposed CUF-1D method is presented in Table 29, where the natural frequencies of B3Dw [32], BC2CM[19] methods, as well as Abaqus shell model, are also compared.

Table 27: First 40 mode shapes of beam 4, 20B4-26L9 model with clamped-free edge conditions

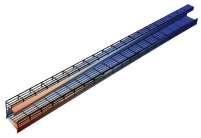 Mode 1	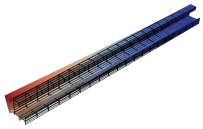 Mode 2	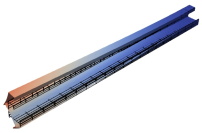 Mode 3	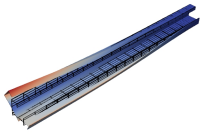 Mode 4	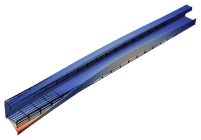 Mode 5
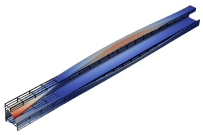 Mode 6	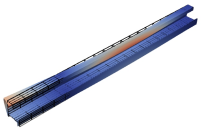 Mode 7	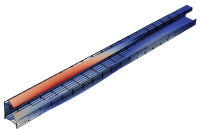 Mode 8	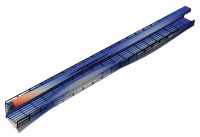 Mode 9	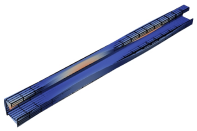 Mode 10
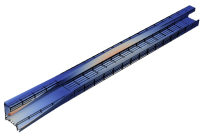 Mode 11	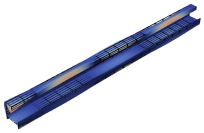 Mode 12	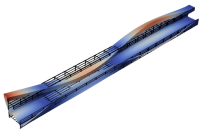 Mode 13	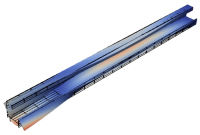 Mode 14	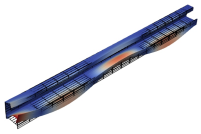 Mode 15
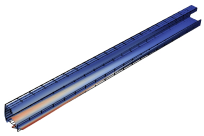 Mode 16	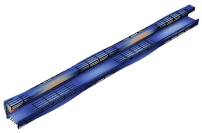 Mode 17	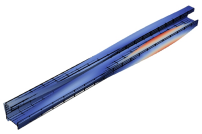 Mode 18	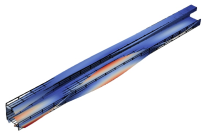 Mode 19	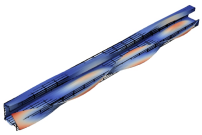 Mode 20
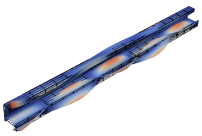 Mode 21	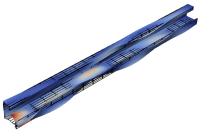 Mode 22	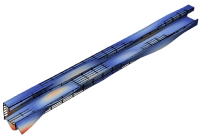 Mode 23	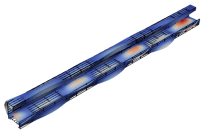 Mode 24	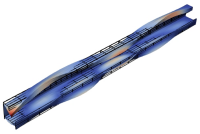 Mode 25
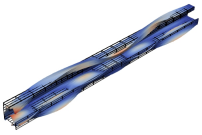 Mode 26	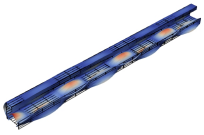 Mode 27	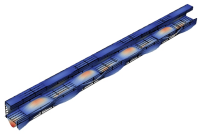 Mode 28	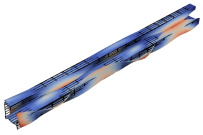 Mode 29	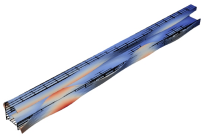 Mode 30
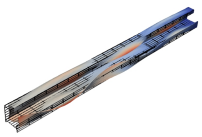 Mode 31	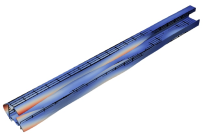 Mode 32	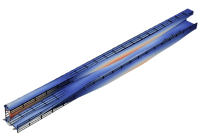 Mode 33	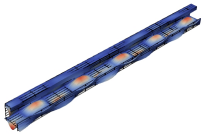 Mode 34	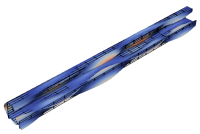 Mode 35
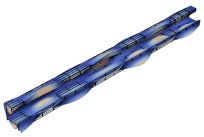 Mode 36	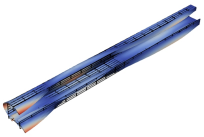 Mode 37	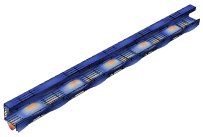 Mode 38	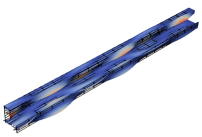 Mode 39	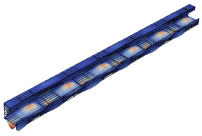 Mode 40

Table 28: The details of Abaqus shell model used for the simulation of beam 4. CUF DOF = 29097.

Model	DOF	number of elements	Element type	Beam axis elements	Cross-Section discretization
Shell	60498	3280	Quadratic S8R	80	41

Table 29: Natural frequencies of beam 4 with clamped-free edge conditions based on different structural theories for the corresponding mode shapes using MAC

Modes	20B4-26L9	20B4,TE=1	20B4,TE=2	20B4,TE=5	20B4,TE=10	20B4-13L9	20B4-17L9	Abaqus shell	B3Dw[32]	BC2CM[19]
Mode 1	3.15	-	-	-	3.93	3.15	3.15	3.13	3.17	3.17
Mode 2	5.71	-	-	-	5.80	5.71	5.71	5.71	5.77	5.77
Mode 3	12.27	-	-	-	-	12.36	12.30	12.17	13.46	13.46
Mode 4	16.04	-	-	-	-	-	16.10	15.81	17.88	17.88
Mode 5	16.22	-	-	-	-	-	16.26	16.04	35.86	35.86
Mode 6	25.34	-	-	-	46.80	25.71	25.56	25.12	49.01	49.02
Mode 7	29.33	-	-	-	-	29.95	29.73	29.03	81.01	81.01
Mode 8	38.76	-	-	-	-	-	-	37.83	95.34	95.34
Mode 9	38.81	-	-	-	-	-	-	38.38	99.47	99.47
Mode 10	42.80	-	-	-	-	44.79	44.26	42.01	128.07	128.10
Mode 11	47.36	-	-	-	-	49.36	48.94	46.61	156.71	156.74
Mode 12	56.71	-	-	-	-	58.54	58.07	55.97	192.44	192.45
Mode 13	59.38	-	-	-	-	60.17	59.86	59.03	216.83	216.83
Mode 14	69.87	-	-	-	-	71.70	70.30	69.02	232.78	232.87
Mode 15	71.76	-	-	-	-	74.07	72.44	70.68	-	-
Mode 16	76.22	-	-	-	-	83.12	77.40	74.18	-	-
Mode 17	77.38	-	-	-	100.23	79.17	78.18	76.64	-	-
Mode 18	82.61	-	-	-	-	88.14	83.64	80.97	-	-
Mode 19	85.58	-	-	-	-	91.35	86.64	83.86	-	-
Mode 20	90.67	-	-	-	-	96.93	92.11	88.82	-	-
Mode 21	94.83	-	-	-	-	-	96.45	92.97	-	-
Mode 22	97.56	-	-	-	-	-	98.92	95.86	-	-
Mode 23	98.57	-	-	-	-	-	99.99	97.49	-	-
Mode 24	107.55	-	-	-	-	-	109.74	105.04	-	-
Mode 25	114.04	-	-	-	-	-	-	111.84	-	-
Mode 26	114.39	-	-	-	-	-	-	112.19	-	-
Mode 27	116.88	-	-	-	-	-	119.98	113.58	-	-
Mode 28	125.30	-	-	-	-	-	-	121.35	-	-
Mode 29	127.87	-	-	-	-	-	-	125.11	-	-
Mode 30	128.05	-	-	-	-	-	-	125.62	-	-
Mode 31	128.29	-	-	-	-	-	-	126.20	-	-
Mode 32	128.50	-	-	-	-	-	-	127.21	-	-
Mode 33	130.44	-	-	-	-	144.37	133.16	128.19	-	-
Mode 34	133.23	-	-	-	-	-	137.62	129.01	-	-
Mode 35	136.60	-	-	-	-	-	139.24	133.35	-	-
Mode 36	137.99	-	-	-	-	-	140.94	134.54	-	-
Mode 37	138.58	-	-	-	-	-	141.37	135.37	-	-
Mode 38	140.75	-	-	-	-	-	146.12	135.61	-	-
Mode 39	147.01	-	-	-	-	160.91	149.77	142.60	-	-
Mode 40	148.43	-	-	-	-	-	154.36	143.71	-	-

The following comments could be made based on the mentioned results:

1. In the higher-order modes, the effect of the adopted structural theory is more significant. For example, see Fig. 20 where the MAC analysis shows some differences between the mode shapes in the higher modes (modes 30-40) for the 20B4-8L9 and 20B4-14L9 models.

2. The proposed CUF-based approach can predict the natural frequencies in good agreement with the more expensive shell-2D models.

3. The obtained results by the CUF refined models reveal the fact that by the proposed method, the mode shapes of the structure are captured reliably with the cross-sectional deformations.

4. As the complexity of the cross-section of the beam is increased, the MAC analysis shows the fact that higher TE is needed in order to capture the accurate mode shapes with the cross-

sectional deformations, For instance, in the beam cases of 3 and 4 with arbitrary sections, most of the models with classical and low order TEs are not capable of finding the accurate mode shapes (See Tables 25 and 29)

5. The obtained results by the CUF refined models confirm the fact that by the proposed method, the mode shapes of the structure are captured reliably with the cross-sectional deformations.

6. For the sake of comparison, the natural frequencies by the methods of B3Dw [32] and BC2CM[19] are compared with the 20B4, TE=2 CUF model.

7 Conclusions

In this study, higher-order vibration modes have been analyzed in a series of open-section thin-walled beams, which had been proposed previously as benchmark problems. The CUF FEs based on the power of cross-sectional deformation coordinates (x, z) and those based on the Lagrangian polynomials have been implemented. A comprehensive comparison has been presented between the classical beam theories, refined ones based on the CUF, shell results by the commercial FE software, and the data available from the literature. The results have demonstrated the reliability and accuracy of the CUF-based approach proposed for the higher-order free vibration analysis of thin-walled beams due to the cross-sectional deformations. The natural frequencies and mode shapes obtained by the proposed efficient method have shown good agreement with the shell models that need considerably higher computational efforts.

The need for the models capable of detecting the cross-sectional deformations has been outlined. In fact, classical beam theories and the linear TE of order one have not been capable of capturing many cross-sectional deformations related to the bending or torsion; instead, they have shown rigid cross-section modes that did not really exist. Global vibration modes, such as bending and torsion, related to the rigid cross-sectional deformations, have been detected via classical and shear refined theories. However, cross-sectional deformations have appeared at higher frequencies, and these modes have been mixed with the global ones. The MAC has been used in order to compare the free vibration modes based on the different structural theories. It has been confirmed that in the higher-order modes, the effect of the adopted structural theory is more significant. In addition, the MAC analysis reveals that more refinement is essential for the TE when used for the complex geometries of the cross-section.

References

[1] A. H. Nayfeh and P. F. Pai. *Linear and nonlinear structural mechanics*. John Wiley & Sons, 2008.

[2] Leonhard Euler. Additamentum i: De curvas elasticis. *Leonhardi Euleri Opera omnia*, 1(24):231–297, 1911.

[3] DANIEL Bernoulli. De vibrationibus et sono laminarum elasticarum. *Commentarii Academiae Scientiarum Imperialis Petropolitanae*, 13(1741-3):105–20, 1751.

[4] Stephen P Timoshenko. Lxvi. on the correction for shear of the differential equation for transverse vibrations of prismatic bars. *The London, Edinburgh, and Dublin Philosophical Magazine and Journal of Science*, 41(245):744–746, 1921.

[5] Stephan P Timoshenko. X. on the transverse vibrations of bars of uniform cross-section. *The London, Edinburgh, and Dublin Philosophical Magazine and Journal of Science*, 43(253):125–131, 1922.

[6] V. Z. Vlasov. Thin-walled elastic beams. *PST Catalogue*, 428, 1959.

[7] V. Z. Vlasov. Thin-walled elastic rods. *Fizmatgiz, Moscow*, 1959.

[8] Xiangyang Xu, Nasim Fallahi, and Hao Yang. Efficient cuf-based fem analysis of thin-wall structures with lagrange polynomial expansion. *Mechanics of Advanced Materials and Structures*, pages 1–22, 2020.

[9] JW Jaworski and EH Dowell. Free vibration of a cantilevered beam with multiple steps: Comparison of several theoretical methods with experiment. *Journal of sound and vibration*, 312(4-5):713–725, 2008.

[10] Suming Xu and Xinwei Wang. Free vibration analyses of timoshenko beams with free edges by using the discrete singular convolution. *Advances in Engineering Software*, 42(10):797–806, 2011.

[11] Myung-Soo Choi, Takahiro Kondou, and Yasuhiro Bonkobara. Development of free vibration analysis algorithm for beam structures by combining sylvester's inertia theorem and transfer stiffness coefficient method. *Journal of mechanical science and technology*, 26(1):11–19, 2012.

[12] D.J. Gorman. *Free Vibration Analysis of Beams and Shafts*. A Wiley-Interscience publication. Wiley, 1975.

[13] Robert D Blevins. Formulas for natural frequency and mode shape. 1979.

[14] SK Jang and CW Bert. Free vibration of stepped beams: exact and numerical solutions. *Journal of sound and vibration*, 130(2):342–346, 1989.

[15] SK Jang and CW Bert. Free vibration of stepped beams: higher mode frequencies and effects of steps on frequency. *Journal of sound and vibration*, 132(1):164–168, 1989.

[16] MJ Maurizi and PM Belles. Free vibration of stepped beams elastically restrained against translation and rotation at one end. *Journal of sound and vibration*, 163(1):188–191, 1993.

[17] F Ju, HP Lee, and KH Lee. On the free vibration of stepped beams. *International journal of solids and structures*, 31(22):3125–3137, 1994.

[18] Wen L Li. Free vibrations of beams with general boundary conditions. *Journal of Sound and Vibration*, 237(4):709–725, 2000.

[19] Hong Hu Chen and Kuo Mo Hsiao. Quadruply coupled linear free vibrations of thin-walled beams with a generic open section. *Engineering Structures*, 30(5):1319–1334, 2008.

[20] Li Jun, Shen Rongying, Hua Hongxing, and Jin Xianding. Coupled bending and torsional vibration of axially loaded bernoulli–euler beams including warping effects. *Applied Acoustics*, 65(2):153–170, 2004.

[21] F Mohri, L Azrar, and M Potier-Ferry. Vibration analysis of buckled thin-walled beams with open sections. *JSV*, 275(1-2):434–446, 2004.

[22] Aleksandar Prokić. On triply coupled vibrations of thin-walled beams with arbitrary cross-section. *Journal of Sound and Vibration*, 279(3-5):723–737, 2005.

[23] Palash Dey and S Talukdar. Influence of warping on modal parameters of thin-walled channel section steel beam. *Procedia Engineering*, 144:52–59, 2016.

[24] Justin Murin, Mehdi Aminbaghai, Juraj Hrabovsky, Giuseppe Balduzzi, Michael Dorn, and Herbert A Mang. Torsional warping eigenmodes of fgm beams with longitudinally varying material properties. *Engineering Structures*, 175:912–925, 2018.

[25] Richardt Schardt. Generalized beam theory—an adequate method for coupled stability problems. *Thin-walled structures*, 19(2-4):161–180, 1994.

[26] Nuno Silvestre and Dinar Camotim. Generalized beam theory to analyze the vibration of open-section thin-walled composite members. *Journal of Engineering Mechanics*, 139(8):992–1009, 2013.

[27] Cilmar Basaglia, Dinar Camotim, and Humberto Breves Coda. Generalised beam theory (gbt) formulation to analyse the vibration behaviour of thin-walled steel frames. *Thin-Walled Structures*, 127:259–274, 2018.

[28] Rui AS Bebiano, Dinar RZ Camotim, and Rodrigo M Gonçalves. Local and global vibration analysis of thin-walled members subjected to internal forces–application of generalised beam theory.

[29] St. Kugler, PA Fotiu, and J. Murin. Analysis of shells, plates, and beams: A state of the art report [ch. beam dynamics using a generalized beam theory based on the solution of a reference beam problem]. 2020.

[30] St. Kugler, PA Fotiu, and J. Murin. A novel gbt-formulation for thin-walled fgm-beam-structures based on a reference beam problem. *Composite Structures*, 257:113158, 2021.

[31] G Piana, E Lofrano, A Manuello, and G Ruta. Natural frequencies and buckling of compressed non-symmetric thin-walled beams. *Thin-Walled Structures*, 111:189–196, 2017.

[32] Wassim Jrad. *Dynamic behavior of thin-walled beams: Analytical, numerical and experimental approaches*. PhD thesis, Université de Lorraine, 2019.

[33] Wassim Jrad, Foudil Mohri, Guillaume Robin, El Mostafa Daya, and Jihad Al-Hajjar. Analytical and finite element solutions of free and forced vibration of unrestrained and braced thin-walled beams. *Journal of Vibration and Control*, 26(5-6):255–276, 2020.

[34] Fiorenzo A Fazzolari. A beam formulation with 3d capabilities for the free vibration analysis of thin-walled metallic and composite structures. *Thin-Walled Structures*, 146:106441, 2020.

[35] RS Langley and NS Bardell. A review of current analysis capabilities applicable to the high frequency vibration prediction of aerospace structures. *The Aeronautical Journal*, 102(1015):287–297, 1998.

[36] GW Wei, YB Zhao, and Yang Xiang. A novel approach for the analysis of high-frequency vibrations. *Journal of Sound and Vibration*, 257(2):207–246, 2002.

[37] Praneeth Reddy Sudalagunta, Cornel Sultan, Rakesh K Kapania, Layne T Watson, and Pradeep Raj. Accurate computing of higher vibration modes of thin flexible structures. *AIAA Journal*, 54(5):1704–1718, 2016.

[38] Jun-lei Ding, Rong-xing Wu, Ji Wang, Long-tao Xie, and Jian-ke Du. A new theory for high frequency vibrations of beams from displacements of trigonometric functions of thickness. In *2017 Symposium on Piezoelectricity, Acoustic Waves, and Device Applications (SPAWDA)*, pages 372–379. IEEE, 2017.

[39] Zhili Lin, Xiliang Chen, and Bo Zhang. Energy finite element analysis of vibrating beams at high frequency. In *2017 IEEE International Conference on Information and Automation (ICIA)*, pages 1033–1038. IEEE, 2017.

[40] Xinwei Wang. Novel discrete singular convolution for high-frequency vibration analysis of structural elements. *AIAA Journal*, 55(12):4364–4375, 2017.

[41] S Brischetto and E Carrera. Free vibration analysis for layered shells accounting of variable kinematic and thermo-mechanical coupling. *Shock and Vibration*, 19(2):151–169, 2012.

[42] Alberto Varello and Erasmo Carrera. Free vibration response of thin and thick nonhomogeneous shells by refined one-dimensional analysis. *Journal of Vibration and Acoustics*, 136(6), 2014.

[43] Maria Cinefra, Stefano Valvano, and Erasmo Carrera. A layer-wise mitc9 finite element for the free-vibration analysis of plates with piezo-patches. *International Journal of Smart and Nano Materials*, 6(2):85–104, 2015.

[44] E Zappino, T Cavallo, and E Carrera. Free vibration analysis of reinforced thin-walled plates and shells through various finite element models. *Mechanics of Advanced Materials and Structures*, 23(9):1005–1018, 2016.

[45] E Carrera, M Petrolo, and P Nali. Unified formulation applied to free vibrations finite element analysis of beams with arbitrary section. *Shock and Vibration*, 18(3):485–502, 2011.

[46] E Carrera, F Miglioretti, and M Petrolo. Computations and evaluations of higher-order theories for free vibration analysis of beams. *Journal of Sound and Vibration*, 331(19):4269–4284, 2012.

[47] M Petrolo, E Zappino, and E Carrera. Refined free vibration analysis of one-dimensional structures with compact and bridge-like cross-sections. *Thin-Walled Structures*, 56:49–61, 2012.

[48] A Pagani, M Boscolo, JR Banerjee, and E Carrera. Exact dynamic stiffness elements based on one-dimensional higher-order theories for free vibration analysis of solid and thin-walled structures. *Journal of Sound and Vibration*, 332(23):6104–6127, 2013.

[49] Alfonso Pagani, Francesco Zangallo, and Erasmo Carrera. Influence of non-structural localized inertia on free vibration response of thin-walled structures by variable kinematic beam formulations. *Shock and Vibration*, 2014, 2014.

[50] A Pagani, E Carrera, and AJM Ferreira. Higher-order theories and radial basis functions applied to free vibration analysis of thin-walled beams. *Mechanics of Advanced Materials and Structures*, 23(9):1080–1091, 2016.

[51] Min Dan, Alfonso Pagani, and Erasmo Carrera. Free vibration analysis of simply supported beams with solid and thin-walled cross-sections using higher-order theories based on displacement variables. *Thin-Walled Structures*, 98:478–495, 2016.

[52] Erasmo Carrera, Maria Cinefra, Marco Petrolo, and Enrico Zappino. *Finite element analysis of structures through unified formulation*. John Wiley & Sons, 2014.

[53] K. J. Bathe. *Finite Element Procedure*. Prentice Hall, Upper Saddle River, New Jersey, USA, 1996.

[54] Erasmo Carrera and Enrico Zappino. Carrera unified formulation for free-vibration analysis of aircraft structures. *AIAA Journal*, 54(1):280–292, 2016.

[55] E. Carrera, A. Pagani, and M. Petrolo. Classical, refined and component-wise theories for static analysis of reinforced-shell wing structures. *AIAA Journal*, 51(5):1255–1268, 2013.

[56] Alfonso Pagani, Ehsan Daneshkhah, Xiangyang Xu, and Erasmo Carrera. Evaluation of geometrically nonlinear terms in the large-deflection and post-buckling analysis of isotropic rectangular plates. *International Journal of Non-Linear Mechanics*, 121:103461, 2020.

[57] E. Carrera, A. Pagani, and M. Petrolo. Refined 1D finite elements for the analysis of secondary, primary, and complete civil engineering structures. *Journal of Structural Engineering*, 141:04014123/1–14, 2015.

[58] E. Carrera and A. Pagani. Free vibration analysis of civil engineering structures by component-wise models. *Journal of Sound and Vibration*, 333(19):4597–4620, 2014.

[59] JN Reddy. On locking-free shear deformable beam finite elements. *Computer methods in applied mechanics and engineering*, 149(1-4):113–132, 1997.

[60] E Carrera, G Giunta, P Nali, and M Petrolo. Refined beam elements with arbitrary cross-section geometries. *Computers & structures*, 88(5-6):283–293, 2010.

[61] OC Zienkiewicz, RL Taylor, and JM0253 Too. Reduced integration technique in general analysis of plates and shells. *International Journal for Numerical Methods in Engineering*, 3(2):275–290, 1971.

[62] OC Zienkiewicz and E Hinton. Reduced integration, function smoothing and non-conformity in finite element analysis (with special reference to thick plates). *Journal of the Franklin Institute*, 302(5-6):443–461, 1976.

[63] David S Malkus and Thomas JR Hughes. Mixed finite element methods—reduced and selective integration techniques: a unification of concepts. *Computer Methods in Applied Mechanics and Engineering*, 15(1):63–81, 1978.

[64] Thomas JR Hughes, Martin Cohen, and Medhat Haroun. Reduced and selective integration techniques in the finite element analysis of plates. *Nuclear Engineering and design*, 46(1):203–222, 1978.

[65] Eduardo N Dvorkin and Klaus-Jürgen Bathe. A continuum mechanics based four-node shell element for general non-linear analysis. *Engineering computations*, 1984.

[66] Richard H Macneal. Derivation of element stiffness matrices by assumed strain distributions. *Nuclear Engineering and Design*, 70(1):3–12, 1982.

[67] E Carrera, AG de Miguel, and A Pagani. Extension of mitc to higher-order beam models and shear locking analysis for compact, thin-walled, and composite structures. *International Journal for Numerical Methods in Engineering*, 112(13):1889–1908, 2017.

[68] Randall J Allemang and David L Brown. A correlation coefficient for modal vector analysis. In *Proceedings of the 1st international modal analysis conference*, volume 1, pages 110–116. SEM Orlando, 1982.

[69] Randall J Allemang. The modal assurance criterion–twenty years of use and abuse. *Sound and vibration*, 37(8):14–23, 2003.

[70] Miroslav Pastor, Michal Binda, and Tomáš Harčarik. Modal assurance criterion. *Procedia Engineering*, 48:543–548, 2012.